Marine Geology 436 (2021) 106457

Contents lists available at ScienceDirect

Marine Geology

journal homepage: www.elsevier.com/locate/margo

Research article

Depositional environments and sequence stratigraphy of post-last glacial maximum incised valley-fill, Malay Basin, northern Sunda Shelf

Michael R. Twarog [a], Stephen J. Culver [a,*], David J. Mallinson [a], Eduardo Leorri [a], Bailey Donovan [a], Emily I. Harrison [a], Haley Hindes [a], Devon Reed [a], Eric Horsman [a], Noor Azhar Mohd Shazili [b], Peter R. Parham [c,d]

[a] Department of Geological Sciences, East Carolina University, 101 Graham Building, Greenville, NC 27858, USA
[b] Institute of Oceanography and Environment, University Malaysia Terengganu, 21030 Kuala Terengganu, Terengganu, Malaysia
[c] US Army Corps of Engineers, Albuquerque District, 287 Bell Ranch Rd., Conchas, NM 88416, USA
[d] Centre of Tropical Geoengineering, Universiti Teknologi Malaysia, Jalan Universiti, 80990 Johor Bahru, Johor, Malaysia

ARTICLE INFO

Keywords:
Sunda Shelf
Late Quaternary
Micropaleontology (forams)
Shelf paleoenvironments
Chronostratigraphy
Sequence stratigraphy

ABSTRACT

The alternating submergence and subaerial exposure of the low-gradient, shallow Sunda Shelf of southeast Asia during Quaternary interglacial-glacial cycles played an important role in ocean circulation and monsoonal climate through the interchange of Indian Ocean and Pacific Ocean waters. The Quaternary stratigraphic development of this margin is, however, poorly understood. This study uses a multi-proxy approach (AMS radiocarbon, bulk sediment magnetic susceptibility, X-ray fluorescence spectrometry, and foraminiferal assemblage data) to characterize environmental change and late Pleistocene to Holocene sequence stratigraphic architecture in 16 cores from the northern Sunda Shelf off the east coast of Peninsular Malaysia.

Five chronostratigraphic units are recognized. Unit 1 is an inner shelf deposit dating from a late Pleistocene sea-level highstand (the highstand systems tract of the pre-LGM base-level cycle). Units 2–4 represent different paleoenvironmenal components of the transgressive systems tract (TST) of the most recent base-level cycle. Unit 2 is a late Pleistocene shallow open embayment deposit that formed during the post-LGM inundation of the paleo-Chao Phraya River valley as sea level rose. Unit 3 is composed of late Pleistocene to early Holocene paralic peat and organic-rich mud and is capped by a transgressive ravinement surface. Unit 4 is a shallow shelf unit deposited during the early Holocene transgression on the Sunda Shelf prior to ca. 6500 cal yr BP (the onset of the regional Holocene sea-level highstand). Unit 5 represents the mid-Holocene to recent highstand systems tract (HST) deposited from ca. 6500 cal yr BP to present.

The incised paleovalleys of the paleo-Chao Phraya River and its tributaries provide more accommodation space for sediment accumulation than the surrounding shelf. However, the thinness of the Holocene sedimentary record, 2–3 m in the incised valleys compared to <1 m over the adjacent shelf, indicates that the LGM incised valleys were almost filled by fluvial and coastal plain sediments before open marine conditions returned near the beginning of the Holocene. The multi-proxy approach of this study elucidates the geologic response of this shelf to sea-level rise and the sequence stratigraphic development of tropical, siliciclastic-dominated shallow shelf depositional sequences.

1. Introduction

At ca. 125,000 km^2, the Sunda Shelf (Fig. 1A) is one of the largest epicontinental shelves in the world (Hanebuth et al., 2000; Alqahtani et al., 2015). It is located within the SE Asian monsoonal system and surrounded by highlands drained by rivers carrying extremely large sediment loads (Milliman et al., 1999). Alternating exposure and submergence of the shelf during glacial-interglacial cycles played an important role in the interchange of Indian Ocean and Pacific Ocean waters and thus ocean circulation and monsoonal climate during the late Quaternary (Wang et al., 1995; Wang et al., 1999). Despite this regional paleoclimatic and paleoceanographic importance, characterization of

* Corresponding author.
E-mail address: culvers@ecu.edu (S.J. Culver).

https://doi.org/10.1016/j.margeo.2021.106457
Received 18 November 2020; Received in revised form 15 February 2021; Accepted 25 February 2021
Available online 1 March 2021

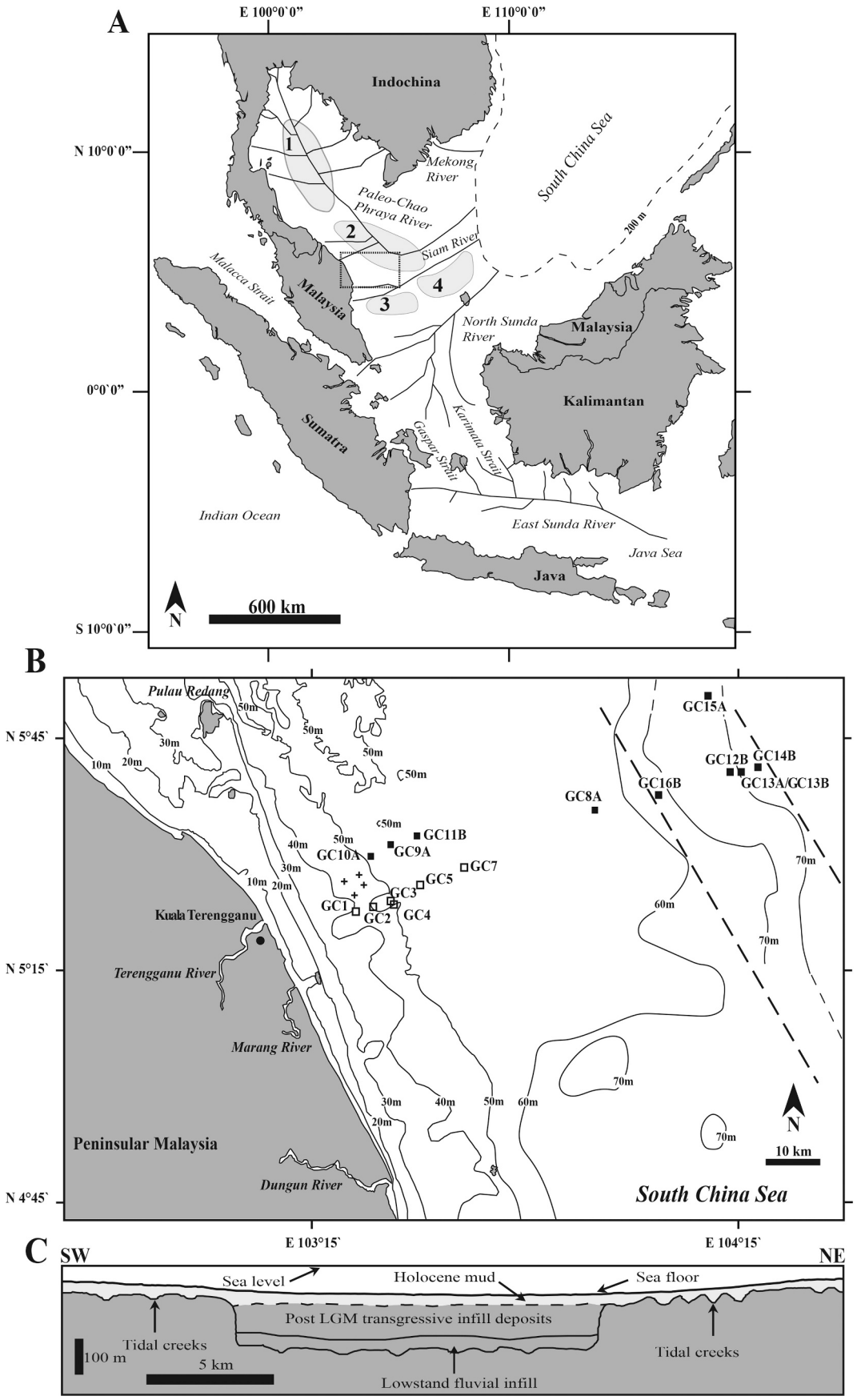

(caption on next page)

Fig. 1. A: Location of the study area (open rectangle) on the Sunda Shelf, southern SCS. The northeastern edge of the Sunda Shelf is indicated by the dashed line. Depositional basins (mainly Neogene-age) from Alqahtani et al. (2017): 1, Pattani; 2 Malay; 3, Penyu; 4, West Natuna. B: Bathymetric map of the shelf off Kuala Terengganu showing locations of cores used in this study (squares) along trends of the paleo-Terengganu and paleo-Marang River systems (tributaries of the paleo-Chao Phraya River). Filled squares indicate the cores investigated for benthic foraminiferal assemblages. Crosses indicate test cores (containing <50 cm of Holocene sediment) taken on the interfluve between the trends of the paleo-Marang and paleo-Terengganu incised valleys. The general location of the paleo-Chao Phraya River incised valley (Alqahtani et al., 2015) is constrained between the dashed lines bracketing the 70 m isobath. C: Cross-sectional depositional model of the paleo-Chao Phraya River incised valley (modified from Alqahtani et al., 2015) ~25 km north of the current study area. Vertical scale is approximated, and exaggerated roughly 15 times. Holocene sediment was interpreted to be 15–18 m thick within the paleo-valley (Alqahtani et al., 2015).

late Quaternary sediments on the Sunda Shelf is largely limited to a transect of cores collected on the central to outer shelf along the trend of the paleo-North Sunda River (Fig. 1A) incised valley (e.g., Hanebuth et al., 2000, 2011; Hanebuth and Stattegger, 2003).

The northern Sunda Shelf and southwestern South China Sea (SCS) are located north of the equator, south of Indochina and to the west and southwest of the deep SCS basin (Fig. 1A). Much of the Sunda shelf was exposed during the last glacial maximum (LGM) sea-level lowstand of ca. −120 m at ca. 26.5 ka to 19 ka (Fairbanks, 1989; Hanebuth and Stattegger, 2003; Clark et al., 2009; Hanebuth et al., 2009). During the LGM, rivers drained across and incised the subaerially exposed shelf, eventually feeding into the semi-enclosed SCS (Hanebuth et al., 2000; Voris, 2000; Sathiamurthy and Voris, 2006). Extensive LGM and post-LGM fluvial and paralic sedimentation within incised valleys prevented the accumulation of thick sections of open marine shelf sediments during post-LGM sea-level rise regionally (e.g., Puchala et al., 2011; Alqahtani et al., 2015, 2017) and in other parts of the globe (e.g., the Gulf of Mexico, Simms et al., 2006; the Bay of Vilaine, Sorrel et al., 2010). Holocene sediments in the incised channels of the North Sunda River consist entirely of mangrove peat or delta front sediments (Hanebuth et al., 2011). Across the open eastern Sunda Shelf at central shelf depths (ca. 70–100 m) Holocene marine sediment consists of <1 m of carbonate-rich mud (Hanebuth et al., 2011). Several other workers have recorded or estimated 2–29 m of Holocene marine mud within incised valleys on the Sunda Shelf (Posamentier, 2001; Miall, 2002; Darmadi et al., 2007; Reijenstein et al., 2011; Puchala et al., 2011; Rahman et al., 2016). Most recently and most relevant to this study, Alqahtani et al. (2015, 2017) posited the existence of a ca. 15–18 m-thick Holocene marine sediment record within the main incised valley of the paleo-Chao Phraya – Johore River (herein referred to as the paleo-Chao Phraya River) in the central Malay Basin (Fig. 1A and C).

Several recent works have described the stacking pattern and geometry of Pleistocene incised valley-fill (and their component fluvial systems) of the low-gradient Sunda Shelf, as revealed by three-dimensional seismic surveys (Miall, 2002; Darmadi et al., 2007; Reijenstein et al., 2011; Alqahtani et al., 2015, 2017). These studies provide an enhanced understanding of the geometry, connectivity and sequence stratigraphic context of non-marine, gas-productive sand bodies within the Neogene stratigraphic record of the Pattani, Malay, Penyu and West Natuna basins (Fig. 1A) of the western and central Sunda Shelf. Thin, post-LGM marine sediments are briefly mentioned in those works but are characterized further in this paper and can be considered analogous to marine sections within Neogene basinal sequences (e.g., fast subsidence phase (22–11 Ma) and the basin sag phase (8–1.8 Ma) within the Malay Basin; Mansor et al., 2014).

This study seeks to advance the understanding of late Pleistocene to Holocene stratigraphic architecture and evolution of the Sunda Shelf using sediment cores taken on the central shelf across the paleo-Chao Phraya River incised valley (Fig. 1) and on the inner shelf (seaward of the coastal sand prism; Hanebuth et al., 2011) along the trends of the paleo-Marang and paleo-Terengganu river incised valleys, two tributaries of the paleo-Chao Phraya River (Fig. 1B). The occurrence of post-LGM Pleistocene and Holocene sediments within these incised river valleys provides the opportunity to use proxies to investigate the stratigraphic evolution in response to sea-level rise on the inner to central Sunda Shelf. Specific objectives are: (1) to document benthic foraminiferal assemblages and interpret them by comparison with modern benthic foraminiferal assemblages on the Sunda Shelf; (2) to characterize post-LGM sediments and to interpret depositional conditions within the paleo-Chao Phraya River incised valley and two of its tributaries; and (3) to provide a sequence stratigraphic interpretation of the post-glacial infill of the paleo-Chao Phraya River incised valley and its tributaries using sedimentological and foraminiferal data and compare the findings to standard models of incised-valley fill (e.g., Zaitlin et al., 1994; Boyd et al., 2006) and other works.

2. Regional setting

2.1. Geology

The low-gradient (1:9000) Sunda Shelf has an average water depth of 70–80 m and is connected to the Java Sea to the south through the Karimata Strait and Gaspar Strait, and to the Indian Ocean through the Malacca Strait. It is open to the deep SCS basin to the northeast (Pelejero et al., 1999; Woodson et al., 2017) (Fig. 1A). When sea level fell to −120

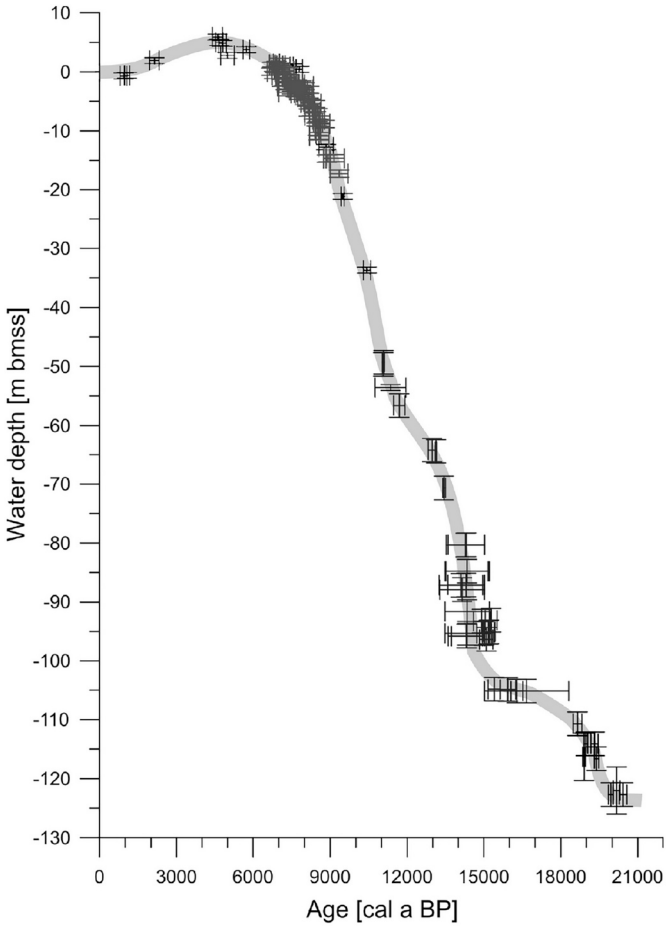

Fig. 2. Sea-level curve for the Sunda Shelf from the LGM to the present day (color removed and reproduced with permission, from Hanebuth et al., 2011). Data for this curve from Geyh et al. (1979), Hesp et al. (1998), Hanebuth et al. (2000), Bird et al. (2007), and Hanebuth et al. (2009).

m during the LGM (Fig. 2) most of the shelf was subaerially exposed and dissected by the Mekong, Siam, North Sunda, East Sunda, and Chao Phraya paleo-rivers and their tributaries (Fig. 1A; see Sathiamurthy and Rahman, 2017, for a review of these river systems). The main trunk of the incised paleo-Chao Phraya River drained southeast across the Gulf of Thailand before turning northeast towards the deep SCS (Fig. 1A), southeast of Indochina (Molengraaff, 1921; Molengraaff and Weber, 1921; Alqahtani et al., 2015, 2017). The incised valleys of the paleo-Terengganu and paleo-Marang rivers drained east-northeast across the Sunda Shelf off the coast of Kuala Terengganu, into the paleo-Chao Phraya River (Fig. 1B). The modern Terengganu River is a low-sinuosity river extending into the hinterland of Malaysia with a catchment area of ca. 5000 km^2. Channel width and depth are ca. 200–400 m and 4–8 m, respectively, near the mouth (Lee et al., 2017). The Marang River is much smaller than the Terengganu and is limited to the coastal plain, with a channel width of ca. 100–150 m. No data could be found on the channel depth. Both rivers exhibit seasonal extremes in discharge and sediment load (both bedload and suspended load) as a result of variable precipitation related to monsoon patterns. Coarse to very coarse sand dominates the bedload of the Terengganu River (Ahmad et al., 2009).

Previous investigations have recognized three late Quaternary stratigraphic units on the Sunda Shelf: a Pleistocene regressive/lowstand unit, a late Pleistocene transgressive unit, and a surficial Holocene unit (e.g., Emmel and Curray, 1982; Evans et al., 1995; Hanebuth and Stattegger, 2003; Sathiamurthy and Rahman, 2017). These units accumulated in response to three major drivers: a change in sea level that prompted a response in sediment deposition; the extent and topography of the Sunda Shelf (i.e., the low relief of the shelf and development of channel structures as a result of fluvial incision); and terrestrial sediment supply (Hanebuth and Stattegger, 2003).

The regressive/lowstand unit was formed during a sea-level fall and lowstand between 50 ka (or older) and 23 ka (Hanebuth and Stattegger, 2003), averages at least 40 m thick, and is composed of marine regressive deposits overlain by terrestrial facies (Hanebuth and Stattegger, 2003). Similar regressive deposits were described by Emmel and Curray (1982) in deltas near the Malacca Strait.

The transgressive unit encompasses a progression of terrestrial to coastal to marine deposits that increase in thickness with present water depth. Age estimates from this unit range from 20.5 to 13 ka, during post-LGM sea-level rise (Hanebuth and Stattegger, 2003). Evans et al. (1995) defined a similar unit largely consisting of channel-fill off southwest peninsular Malaysia. The base of this unit is defined by a subaerial to submarine unconformity (Hanebuth and Stattegger, 2003). 3D multichannel seismic data and lithologic data from drill platform borings compiled by Alqahtani et al. (2015) near the northern margin of our study area reveal that the incised valley of the paleo-Chao Phraya River is 75 m deep and contains several units corresponding to the LGM lowstand and subsequent transgression. The basal unit in the valley consists of gravel and was interpreted as lowstand braided river deposits. These are overlain by marginal marine muds with shells and variable organic material, interbedded sands, inclined heterolithic strata, and a meandering tidally influenced river channel. The uppermost unit was interpreted to be 15–18 m thick and corresponds to Holocene marine muds (Fig. 1C).

The surficial Holocene unit on the eastern Sunda Shelf (Hanebuth and Stattegger, 2003) and northwestern Sunda Shelf (this study) is generally <1 m thick and is composed of foraminifera-rich variably sandy muds. A discontinuity separates this unit from the underlying transgressive unit. Similar thin Holocene units underlain by discontinuities were recorded, for example, by Emmel and Curray (1982), Evans et al. (1995), Reijenstein et al. (2011) and described in cores by Tjallingii et al. (2010) and Puchala et al. (2011).

2.2. Post-LGM sea-level change

The Sunda Shelf region is considered to be tectonically stable (Tjia and Liew, 1996; Michel et al., 2000; Simons et al., 2007) and, thus, the sea-level reconstruction from this region (Fig. 2) is considered to approximate a eustatic curve (Hanebuth et al., 2011). After the LGM lowstand, relative sea level (RSL) rose until ca. 7000 to 6500 cal yr BP when the rate of RSL rise slowed and the Sunda Shelf region experienced a mid-Holocene RSL highstand on the order of +1.3 to +3 m (possibly +5 m) (Hesp et al., 1998; Bird et al., 2007; Hanebuth et al., 2011; Mallinson et al., 2014; Parham et al., 2014; Parham, 2016; Bradley et al., 2016; Fig. 2). Following the mid-Holocene highstand, RSL fell with several possible stillstands in the later Holocene (<5000 cal yr BP; Mallinson et al., 2014; Bradley et al., 2016). Horton et al. (2005) suggested a RSL fall from 4000 to 2000 cal yr BP, likely as a result of hydro-isostatic adjustments. Mallinson et al. (2014) reported similar findings with a RSL fall or stillstand interpreted from ca. 3000 to 1900 cal yr BP. After 1900 cal yr BP, RSL possibly underwent minor oscillations (Mallinson et al., 2014). Yu and Chen (2009) also reported late Holocene oscillations and indicated that RSL was ca. 1.2 m higher than present at 1200 cal yr BP. Approximately 300 cal yr BP, RSL began to rise forming the modern, transgressive system (Mallinson et al., 2014; Culver et al., 2015).

2.3. Foraminifera of the Sunda Shelf

The distribution of foraminifera on the Sunda Shelf is predominantly related to environmental variables that are dependent on water depth and distance from shore (e.g., primary productivity, grain size distribution, calcium carbonate content, salinity and total organic carbon; Szarek et al., 2006; Minhat et al., 2016; Martin et al., 2018; Suriadi et al., 2019; Azmi et al., 2020). Several depth-related zones have been defined on the basis of foraminiferal assemblages (Table 1).

The 0–20 m depth interval is characterized by sandy sediments and by species of the larger benthic foraminifer *Amphistegina*, with several abundant subsidiary taxa off Kuala Terengganu (Table 1; Martin et al., 2018). In contrast, the waters less than 20 m in depth off the southern tip (Johor) of Peninsular Malaysia are characterized by *Elphidium, Pararotalia*, and *Ammonia* (Table 1; Minhat et al., 2016). Martin et al. (2018) recognized three zones off Kuala Terengganu from 20 to 60 m water depth, the two shallower zones are characterized by sandy sediment and strongly dominated by larger benthic foraminifera (Table 1). From ca. 40–60 m water depth, sediments are increasingly muddy, and the assemblage is dominated by *Heterolepa dutemplei* and *Asterorotalia milletti* (Table 1; Martin et al., 2018). Azmi et al. (2020) found similar results offshore of Kelantan, at the Malaysia/Thailand border. In contrast, the assemblage from >20 m water depth, recorded by Minhat et al. (2016), was characterized by agglutinated taxa (e.g., *Bigenerina nodosaria*) in muddy sand substrates (Table 1). Off Sabah, northwest Borneo, Biswas (1976) documented abundant larger foraminifera from 20 to 60 m water depth, similar to assemblages in sandy sediment off Kuala Terengganu (Table 1).

The deepest assemblage recorded by Martin et al. (2018) is dominated by *Heterolepa dutemplei* but also contains relatively abundant specimens of the larger foraminifer, *Assilina ammonoides.* The substrate of these locations is muddy, shell-rich sand. Martin et al. (2018) suggested that this assemblage was likely a mix of modern specimens with older Quaternary specimens (including *Assilina ammonoides)* reworked from underlying sediment by current scour.

The findings of Suriadi et al. (2019), who documented benthic foraminifera from <50 m water depth from Terengganu to Johore, off peninsular Malaysia, were similar to those of Martin et al. (2018). Species of the larger foraminifer *Amphistegina* dominated in sandy substrates whereas *Pseudorotalia schroeteriana* and *Asterorotalia milletti* dominated in muddy substrates (Table 1).

Biswas (1976) recorded two assemblages and Szarek et al. (2006)

Table 1
Foraminiferal assemblages on the Sunda Shelf: Biswas (1976) from several Sunda Shelf locations; Szarek et al. (2006) on the northeastern Sunda Shelf; Martin et al. (2018) on the eastern Sunda Shelf off Kuala Terengganu; Minhat et al. (2016) off Johore, southeastern peninsular Malaysia; and Suriadi et al. (2019) off the east coast of peninsular Malaysia.

Biswas (1976) (>63 μ)	Szarek et al. (2006) (>150 μ)	Minhat et al. (2016) (>63 μ)	Martin et al. (2018) (>150 μ)	Suriadi et al. (2019) (>75 μ)
0–20 m water depth No Planktonics Benthic species richness 33 *Quinqueloculina semistriata* *Elpidium cripsum* *Ammonia beccarii* *Calcarina hispida*		**<20 m water depth** *Elphidium* species *Pararotalia nipponica* *Pararotalia* sp. 1 *Ammonia tepida*	**8–14 m water depth** Sandy substrate Total number of benthic taxa 49 *Amphistegina radiata* (10%) *Amphistegina lessonii* (7%) *Planorbulina acervalis* (6%) *Sahulia conica* (6%) *Millettiana millettii (5%)*	**14–47 m water depth** **Sand substrate** *Amphistegina papillosa* (22%) *Amphistegina lessonii* (8%) *Assilina ammonoides* (8%) *Elphidium crispum* (6%) **Mud substrate** *Pseudorotalia schroeteriana* (10%) *Asterorotalia milletti* (7%) *Elphidium crispum* (6%) *Asterorotalia pulchella* (5%) *Heterolepa dutemplei* (5%) *Cavarotalia annectens* (5%)
20–60 m water depth Benthic species richness ca. 50 to ca. 78 Planktonic foraminifera 5–10% *Quinqueloculina seminulum* *Pseudorotalia schroeterianus* *Cellanthus craticulatus* *Amphistegina lessonii* *Operculina ammonoides* *Operculina venosa*		**>20 m water depth** *Textularia pseudosolita* *Textularia foliacea* *Textularia agglutinans* *Bigenerina nodosaria*	**21–22 m water depth** Sandy substrate Total number of benthic taxa 33 *Amphistegina lessonii* (54%) *Amphistegina radiata* (31%) *Cellanthus craticulatus* (8%)	
		0–40 m water depth *Asterorotalia pulchella* *Cavarotalia annectens* *Pseudorotalia schroeteriana* *Eponides repandus*	**32–41 m water depth** Muddy sand substrate Total number of benthic taxa 46 *Assilina ammonoides* (15%) *Amphistegina radiata* (13%) *Discorbinella bertheloti* (9%) *Amphistegina lessonii* (7%) *Millettiana millettii* (5%)	
			water depths < 60 m Mud substrate ~ 5% planktonics Total number of benthic taxa 50 *Heterolepa dutemplei* (16%) *Asterorotalia milletti* (16%) *Elphidium advenum* (9%) *Ammonia supera* (8%) *Textularia* sp. A (7%).	
60–120 m water depth Benthic species richness 85 Planktonic foraminifera 40% *Spiroloculina communis* *Cibicides margaritiferus* *Cibicides praecinctus* *Cancris indicus*	**Inner shelf (60–109 m water depth)** *Ammomassilina alveoliniformis* *Asterorotalia pulchella* *Neouvigerina proboscidea* *Islandiella japonica* *Hanzawaia nipponica* *Pseudogaudryina pacifica* *Fijinonion fijiense* <7500 individuals/10 cc		**60 m water depth** Sandy mud substrate ~ 5% planktonics Total number of benthic taxa 56 *Heterolepa dutemplei* (18%) *Assilina ammonoides* (9%) *Textularia* sp. A (7%) *Hanzawaia grossepunctata* (6%) *Elphidium advenum* (6%)	

Table 2
Location (decimal degrees), water depth, core length, distance from shoreline, and interval of sediment disturbed by coring.

Core ID	Core location	Water depth (m)	Core length (cm)	Dist. from shore (km)	Interval of disturbed sediment
GC1	5.373°, 103.365°	51.5	200	24	0–16 cm
GC2	5.374°, 103.397°	53.6	200	28	0–32 cm
GC3	5.382°, 103.435°	54.9	300	32	0–6 cm
GC4	5.376°, 103.438°	56	300	32	0–6 cm
GC5	5.419°, 103.483°	58	203	38	0–15 cm
GC7	5.450°, 103.566°	59	164	48	0–10 cm
GC8A	5.585°, 103.930°	59.8	167	90	0–17 cm
GC9A	5.517°, 103.433°	56.5	146	38	0–23 cm
GC10A	5.500°, 103.400°	55.7	192	34	0–34 cm
GC11B	5.533°, 103.483°	57.2	175	43	0–34 cm
GC12B	5.6663°, 104.235°	75	182	126	0–48 cm
GC13A	5.6666°, 104.2605°	73	194	130	0–43 cm
GC13B	5.6666°, 104.2605°	73	190	130	0–35 cm
GC14B	5.6771°, 104.3006°	68	135	134	0–26 cm
GC15A	5.8320°, 104.1839°	77	224	127	0–26 cm
GC16B	5.6163°, 104.0658°	71	215	106	0–46 cm

Location and water depth were recorded using the satellite navigation and depth sounding instruments onboard the *RV Discovery* and *RV Discovery II*. Distance from shoreline was measured using Google Earth.

recorded four assemblages from 60 to 200 m water depth that were not recorded in the shallower waters off Kuala Terengganu (Martin et al., 2018) and the southern tip of peninsular Malaysia (Minhat et al., 2016). Planktonic foraminifera did not occur from 0 to 20 m water depth but then increased in abundance within foraminiferal assemblages from 5–10% to 65–80%, with increasing depth; benthic species richness also increased with depth (Biswas, 1976; Table 1). Szarek et al. (2006) similarly noted increasing diversity of benthic foraminifera and increasing relative abundance of planktonic foraminifera with increasing water depth and distance from shoreline (Table 1). Martin et al. (2018) reported planktonic foraminifera present off Kuala Terengganu in water depths exceeding 30 m and with increasing percentage as both distance from shoreline and water depth increased. Benthic species richness also increased with depth after an initially high value in the shallowest biofacies (CGT1) (8–14 m water depth) (Martin et al., 2018). Minhat et al. (2016) reported that numbers of species were higher in deeper water than shallower water off Johore but her study only documented foraminifera in waters <40 m in depth.

3. Materials and methods

3.1. Core collection, logging and sampling

Sixteen gravity cores (2 m and 3 m barrels with 7 cm internal diameter plastic liners) were collected from the *RV Discovery* and *RV Discovery II* (Universiti Malaysia Terengganu) (Fig. 1B; Table 2). Coring locations were selected by analysis of marine charts, and by using maps in Alqahtani et al. (2015) and unpublished geophysical data off the coast of Kuala Terengganu (Dr. David Menier, personal communication).

The cores were cut in half lengthwise and logged. The gravity coring process disturbed the upper portions (26–48 cm) of each core (Table 2). The remaining sections of each core were cut into 1 cm or 2 cm contiguous samples. The outer ca. 1–2 mm of sediment was scraped from each sample to preclude contamination between samples due to smearing during the coring process. Sediment within large burrows was not sampled.

Depending on the core, samples were taken at 1 cm, 3 cm or 10 cm intervals for analysis of bulk sediment magnetic susceptibility (BMS), at 1 cm, 6 cm, 10 cm or 15 cm intervals for elemental analysis, and at 12 cm or 20 cm intervals for analysis of foraminiferal assemblages (foraminiferal assemblages were not studied in cores GC1, GC2, GC3, GC4, GC5 and GC7). Sampling of the sixteen cores yielded 787 BMS samples, 322 elemental samples, and 99 foraminiferal samples.

3.2. Sediment analysis

3.2.1. Bulk sediment magnetic susceptibility

Magnetic susceptibility analyses were performed using a Kappabridge MFK1-A instrument (Advanced Geoscience Instruments Company - AGICO). Each BMS sample (5.5 cc of dried sediment) was analyzed five times at an induced magnetic field of 200 A/m and a frequency of 976 Hz. Results were averaged to produce a mean value of volume magnetic susceptibility. The MFK1-A was calibrated using a reference standard of known magnetic susceptibility (provided by AGICO) at the beginning and end of each sample run. A reference sample (TER15-GC5, 19.2–20.5 cm) was analyzed every 15 sample runs and the standard deviation of the temporal data series was used as the analytical error ($4.84 \times 10^{-5} \pm 1.91 \times 10^{-6}$; error < 5%). Changes smaller than 5% were considered within the error. Correlation analyses were conducted to determine the relationship between BMS and major elements.

3.2.2. X-ray fluorescence spectrometry

Each sample was analyzed for 19 major and trace elements through a wavelength-dispersive X-ray fluorescence spectrometer. The application used for analysis was constructed using 21 standards from the National Institute of Standards and Technology and the United States Geological Survey. A reference standard (XLSC REF 10.2) was run, at a minimum, during the beginning and end of each analysis session to monitor performance. The error for this analysis is considered to be the root mean square for the calibration of each channel (automated within the software) in conjunction with the standard deviation of the reference sample results.

3.3. Foraminiferal analysis

Foraminiferal samples from 10 of 16 cores were weighed and disaggregated by soaking overnight in a weak solution of sodium hexametaphosphate and sodium hydroxide. Samples were washed over a nest of 1000, 150, and 63 μ sieves to remove the mud fraction and to separate the sand-sized fraction, in which foraminifera were concentrated, from the coarser-sediment fraction. To provide data comparable to that in Szarek et al. (2006) and Martin et al. (2018), 300 specimens per sample from the 150–1000 μ fraction were utilized. Benthic foraminifera were identified to the species level by comparison with illustrations in foraminiferal studies from the South China Sea region (e.g., Graham and Militante, 1959; Whittaker and Hodgkinson, 1979; Haig, 1988; Loeblich Jr. and Tappan, 1987, 1994; Jones, 1994; Szarek, 2001; Culver et al., 2012, 2015; Martin et al., 2018). The percent of planktonic foraminifera was calculated for 12 cores. Identifications of benthic taxa were confirmed by reference to type and comparative material located in the Cushman Collection, Smithsonian Institution, Washington, D.C.

Relative abundances calculated from foraminiferal census data were plotted to exhibit trends of foraminifera in the cores. Species richness (S, number of species in a sample), Fisher's alpha, percent Rotaliina, Miliolina, Textulariina and percent planktonics were determined for each

sample.

Q-mode hierarchical cluster analysis (Mello and Buzas, 1968) was used to distinguish groups within the benthic foraminiferal relative abundance data in 87 samples (samples from GC8A were excluded; see below). Only those species represented by 2% or more of the assemblage in one or more samples were included in the cluster analysis dataset. Relative abundance data were transformed prior to analysis using the equation, 2 arc sin $\sqrt{p_i}$ (Buzas, 1979), where p_i is equal to the fraction of the i^{th} species. All core samples were analyzed together using Ward's linkage and Euclidean distances in SYSTAT 13 (Systat Software Inc., Chicago, Illinois).

3.4. Geochronology

Thirty-nine samples were sent to National Ocean Sciences Accelerator Mass Spectrometry (NOSAMS) in Woods Hole, MA for C-14 AMS radiocarbon dating. Dependent upon specimen availability, samples consisted of the benthic foraminifera *Pseudorotalia indopacifica, Pseudorotalia schroeteriana* or *Cavarotalia annectens*. In two cases, articulated bivalves were dated due to low numbers of foraminifera. One detrital wood sample was also dated. Age estimates for marine shell material were calibrated using the Marine13 calibration curve through CALIB 7.1 (Stuiver et al., 2017). A delta R of −45 with an uncertainty of 49 was used to adjust for regional marine reservoir affects (Southon et al., 2002). The IntCal13 (Calib 7.0 program; Reimer et al., 2013) calibration curve was used for the wood sample.

4. Results

Radiocarbon results and associated lithofacies from the sixteen cores provide the basis for five chronostratigraphic units (Fig. 3; Table 3). These are described below with their associated lithofacies, foraminiferal biofacies, elemental and BMS data (Supplemental Appendices 1–4).

4.1. Unit 1 (late Pleistocene – pre-LGM)

This unit was recovered only in core GC8A (Fig. 4) and is unique in that the radiocarbon ages are very near the limit of radiocarbon dating (>50,000–46,711 and 45,085–42,851 cal yr BP; Table 4). Unit 1 is composed of a burrowed, slightly shelly grey mud lithofacies. Benthic and planktonic foraminifera occur throughout Unit 1 and the latter increase slightly in abundance up-section (Fig. 4). Benthic species diversity is high and generally constant up-section (Table 5). Abundant benthic taxa (Table 3) *Asterorotalia pulchella* and *Hanzawaia nipponica* both increase in abundance up-section and then decrease. *Heterolepa dutemplei* exhibits the reverse trend (Fig. 4). Elemental values show no major trends, except for a slight decrease in Al in the upper 40 cm (Fig. 4). Al has a mean of 16.54 wt% and 1st st. dev. of 1.31; Fe has a mean of 6.54 wt% and 1st st. dev. of 0.34; Ca has a mean of 1.95 wt% and 1st st. dev. of 0.41 (Table 3). BMS has a mean of 1.92×10^{-4} SI units (1 st. dev.: 1.17×10^{-5} SI) (Table 3), and shows no clear trend up-core (Fig. 4).

4.2. Unit 2 (late Pleistocene – post-LGM)

This unit occurs in the base of core GC16B (Fig. 5), where a radiocarbon age of 12,700 ± 119 (Table 4) is associated with a grey mud lithofacies with occasional burrows and shell fragments. Benthic foraminiferal assemblages of this unit are dominated by *Ammonia tepida,* although *Asterorotalia pulchella* occurs in high abundance (~40%) in one sample at the top of the unit. *Heterolepa dutemplei* also occurs in minor amounts. Planktonic foraminifera are absent (Table 3; Fig. 5). Elemental profiles of Al, Fe and Ca are generally constant throughout the unit. (Fig. 5). Al has a mean of 18.26 wt% and 1st st. dev. of 0.68; Fe has a mean of 4.92 wt% and 1st st. dev. of 0.67; Ca has a mean of 0.27 wt% and 1st st. dev. of 0.05 (Table 3). BMS has a mean of 5.06×10^{-5} SI units (1 st. dev.: 1.39×10^{-5} SI) (Table 3) and shows a general increase in susceptibility upward in the core (Fig. 5).

4.3. Unit 3 (late Pleistocene to early Holocene)

Unit 3 was recovered in cores GC1, GC2, GC3, GC4 and GC11B, and GC14B (Figs. 6, 7), and produced ages of 11,570 ± 303 cal yr BP to 11,190 ± 141 (Table 4). This unit is truncated by erosion with a preserved section on the inner shelf, along the trend of the paleo-Marang and paleo-Terrenganu Rivers, and a section farther offshore (the most

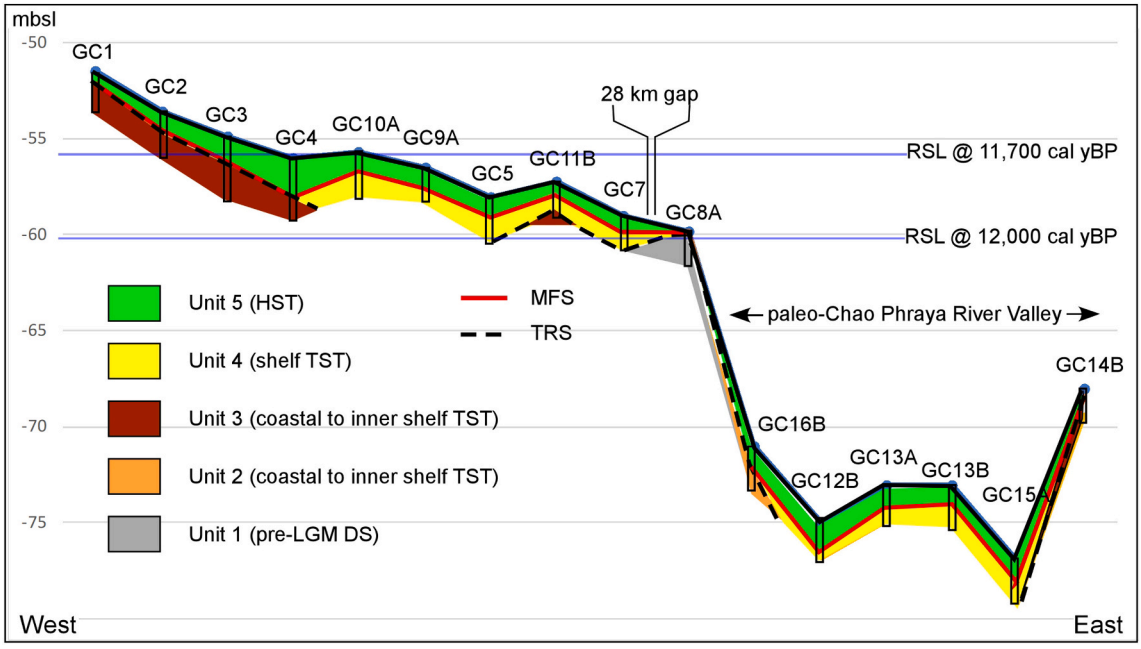

Fig. 3. Cross-section showing the west to east distribution of chronostratigraphic units 1–5. Note that the maximum flooding surface (MFS) and transgressive ravinement surface (TRS) are amalgamated in several cores. The blue lines show the elevation of sea-level at 12,000 cal y BP and 11,700 cal y BP based on data from Hanebuth et al. (2011).

Table 3
Summary of lithological, foraminiferal, BMS, elemental and radiocarbon age data, chronostratigraphic units and their environmental and sequence stratigraphic interpretations.

Chronostratigraphic units and the cores in which they occur	Geographic location	Age range (cal yr BP)	Lithology	BMS	Elements (Al, Fe, Ca)	Benthic foraminiferal assemblage	% Planktonic foraminifera	Interpreted environment	Sequence Strat. Interp.
Unit 5 (cores GC1, GC2, GC3, GC4, GC5, GC7, GC9A, GC10A, GC11B, GC12B, GC13A, GC13B, GC14B, GC15A, GC16B	Along trends of paleo-Marang and paleo-Terengganu rivers and over the paleo-Chao Phraya incised valley.	~6500 to 347 ± 119	Green-grey to brown, shelly, variably sandy (increasing up-core) mud.	BMS values are variable but are generally less than in Unit 4. Mean of means (SI) 7.63E-05; SD 1.05E-05.	Elemental data (Fe, Al and Ca) for the lower 30–50 cm of Unit 5 are more variable than for the overlying portion of the unit. A slight upward increase in Al (and Fe to a lesser degree) is associated with a decrease in Ca, similar to that seen in Unit 4. Mean of means wt% (SD): 13.59 (1.4), 3.83 (0.46) and 12.66 (1.84) for Al, Fe and Ca, respectively.	*Heterolepa dutemplei, Hanzawaia nipponica, Asterorotalia millettii,* and *Textularia* sp. A., are generally the most dominant species. *Cluster group F2A* (furthest offshore), high diversity (57 taxa), highest no. specimens/ 1 g of sediment (max. of 95,335; Table 4), dominated by *Heterolepa dutemplei* (14.65%) and *Textularia* sp. A (13.26%); *Cluster group F3*, low diversity (26 taxa), dominated by *Heterolepa dutemplei* (13.11%), *Asterorotalia milletti* (11.73%), *Textularia* sp. A (9.36%) and *Hanzawaia nipponica* (7.27%).	Planktonics are generally significantly greater in abundance (5.4% mean) than in Unit 4. Max. value of 25% in GC15A.	Inner shelf, 55–60 m water depth to the west and ~ 70 m water depth to the east over the paleo-Chao Phraya valley.	HST
Unit 4 (cores GC5, GC7, CG9A, GC10A, GC11B GC12B, GC13A, GC13B, GC15A)	Along trends of paleo-Marang and paleo-Terengganu rivers and over the paleo-Chao Phraya incised valley.	10,710 ± 179–6490 ± 143	Burrowed, slightly shelly (in layers) grey-green to brown, variably sandy mud. Organic lenses in some cores. Wood fragments near the base where the unit unconformably overlies Unit 3.	Values variable with no consistent trends. Mean of means (SI) 1.12E-04; SD 9.96E-06.	In most cores Al and Fe wt% decrease slightly upward while Ca wt% increases. Mean of means wt% (SD): 16.61 (0.55), 5.14 (0.32) and 3.48 (0.91) for Al, Fe and Ca, respectively.	Benthic foraminiferal assemblages are generally dominated by *Heterolepa dutemplei, Hanzawaia nipponica,* and *Textularia* sp. A., although *Asterorotalia pulchella* dominates in GC11B. *Cluster group F2B* (furthest offshore), high diversity (55 taxa), dominated by *Heterolepa dutemplei, Hanzawaia nipponica, Textularia* sp. A; *Cluster group F1C,* low diversity (20 taxa), dominated by *Asterorotalia pulchella* (30.58%), with *Textularia* cf. *T. agglutinans* (10.26%), *Hanzawaia nipponica* (8.88%), and *Cavarotalia annectens* (7.79%); *Cluster group F3*, low diversity (26 taxa), dominated by *Heterolepa dutemplei* (13.11%), *Asterorotalia milletti* (11.73%), *Textularia* sp. A (9.36%) and *Hanzawaia nipponica* (7.27%).	Planktonics are either absent or rare (2.1% mean) but generally increase slightly in abundance up-core. Max. value of 8.2% in GC13A.	Deepening upward (20–70 m) inner shelf.	TST

(*continued on next page*)

Table 3 (*continued*)

Chronostratigraphic units and the cores in which they occur	Geographic location	Age range (cal yr BP)	Lithology	BMS	Elements (Al, Fe, Ca)	Benthic foraminiferal assemblage	% Planktonic foraminifera	Interpreted environment	Sequence Strat. Interp.
Unit 3 (cores GC1, GC2, GC3, GC4, GC11B, GC14B)	Along trend of paleo-Marang and paleo-Terengganu rivers. Over east margin (left bank) of paleo-Chao Phraya R (GC14B).	11,570 + 303–11,190 + 141	Brown peaty mud. Burrowed, black, organic-rich mud in GC14B.	No data for GC1, GC2, GC3, GC4, GC11B. Values decrease up-core in GC14B. Mean (SI) 2.52E-05; SD 3.39E-06.	No data for GC1, GC2, GC3, GC4, GC11B. %Al and %Fe decrease slightly up-core in GC14B. Means wt% (SD): 13.83 (1.21), 3.67 (0.40) and 0.61 (0.1) for Al, Fe and Ca, respectively.	No forams in GC1, GC2, GC3, GC4, GC11B. *Cluster group F1B*, high diversity (53 taxa), dominated by *Asterorotalia pulchella* (20.6%) and *Heterolepa dutemplei* (10.63%) in GC14B.	No forams in GC1, GC2, GC3, GC4, GC11B. 7.54% mean planktonics in GC14B, negative correlation with *Asterorotalia pulchella*.	Paralic (coastal plain) in.GC1, GC2, GC3, GC4, GC11B. Inner shelf, ~15 m in GC14B	TST
Unit 2 (core GC16B)	Over west margin (right bank) of paleo-Chao Phraya R.	12,700 ± 119	Grey mud with occasional burrows and shell fragments.	Values incease up-core through the unit. Mean (SI) 5.06E-05; SD 1.39E-05	%Al, %Fe and %Ca are generally constant through the unit. Means wt% (SD): 18.26 (0.68), 4.92 (0.67) and 0.27 (0.05) for Al, Fe and Ca, respectively.	*Cluster group F1A*; low diversity (18 taxa); strongly dominated by *Ammonia tepida* (63.8%).	Absent	Shallow shelf <10 m	TST
Unit 1 (GC8A)	Along trend of paleo-Marang and paleo-Terengganu rivers.	[50,000]–46,711 ± 117–43,968 ± 1117	Burrowed, slightly shelly grey mud	Values increase slightly up-core but are highly variable. Mean (SI) 1.92E-04; SD 1.17E-05.	Generally consistent values up-core to 40 cm where %Ca slightly increases and %Al decreases. Means wt% (SD): 16.54 (1.31), 6.54 (0.34) and 1.95 (0.41) for Al, Fe and Ca, respectively.	High diversity (99 taxa); dominated by *Asterorotalia pulchella* (14.14%), *Hanzawaia nipponica* (13.33%).	1.78% (mean); increasing up-core from <1 to 8.5%	Inner shelf (~40–60 m); deepening up-core.	HST (late Pleistocene)

Unit 1 is part of the late Pleistocene base-level cycle and occurs only in GC8A.

seaward recovered core, GC14B). On the inner shelf (cores GC1–4, GC11B; Figs. 6, 7), Unit 3 is characterized by brown peaty mud that is barren of foraminifera. No other data were acquired from this section. Further offshore in GC14B (Fig. 7), the unit consists of a burrowed, black organic-rich mud lithofacies (Table 3). Foraminiferal assemblages in the offshore region are dominated by *Asterorotalia pulchella* and *Heterolepa dutemplei* (Fig. 7). Planktonic foraminifera and *A. pulchella* exhibit a negative correlation. Elemental profiles were measured in core GC14B only. Al and Fe decrease slightly up-core while the Ca profile is constant (Fig. 6). Al has a mean of 13.83 wt% and 1st st. dev. of 1.21; Fe has a mean of 3.67 wt% and 1st st. dev. of 0.4; Ca has a mean of 0.61 wt% and 1st st. dev. of 0.1 (Table 3). BMS was measured in core GC14B only, where susceptibility has a mean of 2.52×10^{-5} SI units (1 st. dev.: 3.39×10^{-6} SI) and decreases slightly upward (Fig. 7).

4.4. Unit 4 (early to middle Holocene)

This Unit was recovered in cores GC5, GC7, GC9A, GC10A, GC11B, GC12B, GC13A, GC13B, and GC15A (Figs. 7–10). Unit 4 radiocarbon ages range from 10,710 ± 179 to 6490 ± 143 (Table 4). The unit is generally characterized by a burrowed, slightly shelly (in layers), grey-green to brown, variably sandy mud lithofacies. Organic lenses occur in some cores, and wood fragments were noted near the base of the unit where it unconformably overlies Unit 3 (GC11B, Fig. 7). Benthic foraminifera occur throughout the unit, whereas planktonics are either absent or rare but generally increase slightly in abundance up-core (GC5, Fig. 9; GC15A, Fig. 10). Benthic foraminiferal assemblages are generally dominated by *Heterolepa dutemplei*, *Hanzawaia nipponica*, and *Textularia* sp. A., although *Asterorotalia pulchella* dominates in GC11B (Table 3; Fig. 7). In most cores that sampled this unit, Al and Fe wt% decrease slightly upward while Ca wt% increases (e.g., GC11B, Fig. 7). Al has a mean of means of 16.61 wt% and 1st st. dev. of 0.55; Fe has a mean of means of 5.14 wt% and 1st st. dev. of 0.32; Ca has a mean of means of 3.48 wt% and 1st st. dev. of 0.91 (Table 3). BMS was measured in all nine cores, and shows no consistent trend upwards; some cores show modest decrease in BMS, while others show a modest increase, or no appreciable change. The mean of means of BMS values for Unit 4 is 1.12×10^{-4} SI units (1 st. dev.: 9.96×10^{-6} SI).

4.5. Unit 5 (middle to late Holocene)

Unit 5 is the uppermost unit throughout the study area, and was recovered in all cores, except GC8A (Figs. 5–10; Table 3). Unit 5 radiocarbon ages range from 6260 ± 93 to 347 ± 119 cal yr BP (Table 4) and is characterized by a greenish-grey to brown, shelly, variably sandy (generally increasing up-section) mud lithofacies. Benthic and planktonic foraminifera occur throughout this unit, and planktonics are generally significantly greater in abundance than in Unit 4. *Heterolepa dutemplei, Hanzawaia nipponica, Asterorotalia millettii, Textularia* sp. A., are the most dominant species, (Table 3; Figs. 5, 8–10). Elemental data (Fe, Al and Ca) for the lower 30–50 cm of Unit 5 are more variable than for the overlying portion of the unit (GC3, Fig. 6; GC4, Fig. 1). A slight upward increase in Al (and Fe to a lesser degree) is associated with a decrease in Ca, similar to that seen in Unit 4. Al has a mean of means of 13.59 wt% and 1st st. dev. of 1.4; Fe has a mean of means of 3.83 wt% and 1st st. dev. of 0.46; Ca has a mean of means of 12.66 wt% and 1st st. dev. of 1.84 (Table 3). BMS was measured in all cores except GC8, and has a mean of means of 7.63×10^{-5} SI units (1 s.d.: 1.05×10^{-5} SI). No consistent trend is apparent upward in the cores, but the mean BMS is lower for Unit 5 than Unit 4 in every core.

4.6. Cluster analysis of benthic foraminiferal relative abundance data

Eighty-seven samples cluster into three major groups (F1, F2 and F3) (Fig. 11). Subdivision of F1 and F2 results in six groups that are summarized below: F1A, F1B, F1C, F2A, F2B, and F3 (Table 6). The

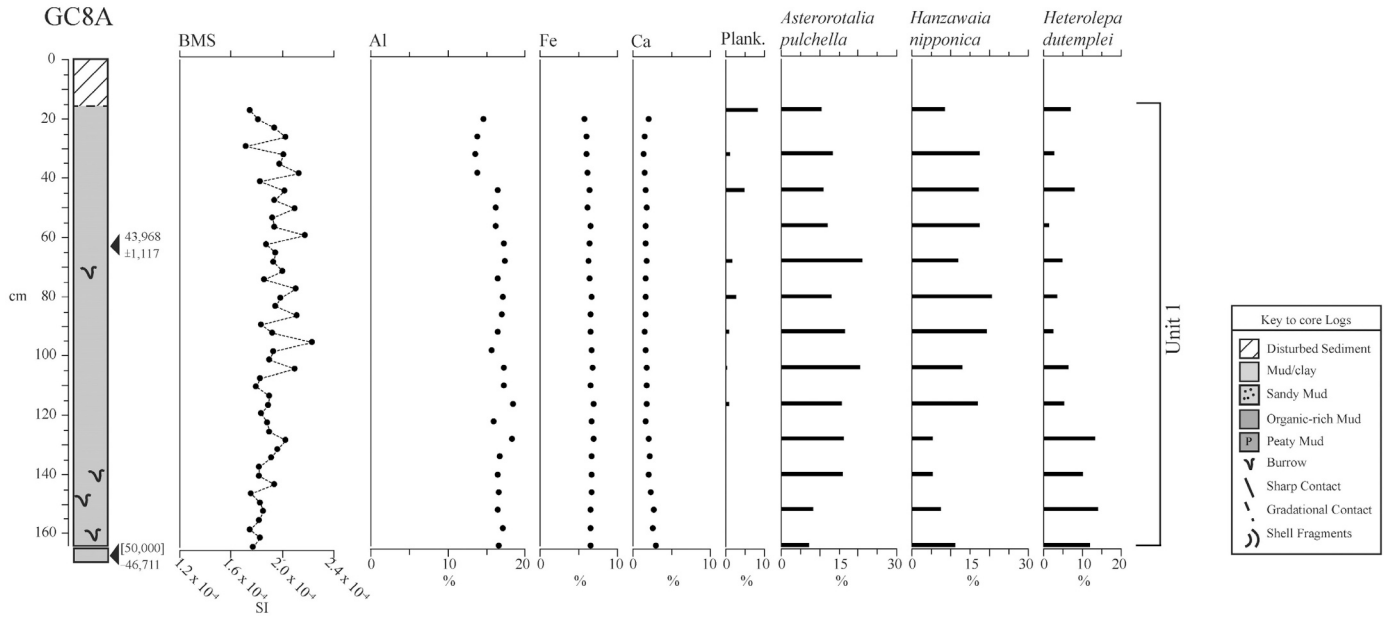

Fig. 4. Lithologic log for core GC8A (59.8 m water depth), composed of chronostratigraphic Unit 1, with radiocarbon age estimates, BMS, Al, Fe, and Ca plots, percent planktonic foraminifera, and relative abundance of the three most abundant benthic foraminiferal species. Key to core log symbols for Figs. 4–10.

distribution of the cluster groups in the cores is shown on the lithologic logs of Figs. 5–10. The analysis did not include samples from an earlier base-level cycle (Unit 1, Core GC8A) (see Discussion).

Low diversity (18 taxa) F1A (Table 6) is strongly dominated by *Ammonia tepida* (63.4%) with *Asterorotalia pulchella* and *Quinqueloculina adiazeta* also contributing significantly (nearly 10% each) to the assemblage (Table 6). F1A characterizes Unit 2 (in GC16B; Fig. 5).

High diversity (53 taxa) F1B is dominated by *Asterorotalia pulchella* (20.6%) and *Heterolepa dutemplei* (10.6%) (Table 6). This cluster group characterizes the marine facies of Unit 3 (Fig. 7; GC14B).

Clustering closer to F1B than F1A (Fig. 11), low diversity (20 taxa) F1C is dominated by *Asterorotalia pulchella* (30.6%) with *Textularia* cf. *T. agglutinans* (10.3%), *Hanzawaia nipponica* (8.9%) and *Cavarotalia annectens* (7.8%) as secondary abundant species (Table 6). This cluster group is found only in core GC11B in Units 4 and 5 (Fig. 7).

High diversity (57 taxa) F2A is co-dominated by *Heterolepa dutemplei* (14.7%) and *Textularia* sp. A (13.3%) (Table 6). This cluster group dominates in the farthest offshore section of Unit 5 (cores GC16B, GC12B, GC13A, GC13B, GC15A: Figs. 5, 9, 10) within the paleo-Chao Phraya River valley (Fig. 3).

High diversity (55 taxa) F2B, clustering with F2A (Fig. 11), has no single dominant taxon; *Heterolepa dutemplei* (11.3%), *Hanzawia nipponica* (9.3%), and *Textularia* sp. A (9.0%) are the most abundant species (Table 6). This cluster group occurs only in Unit 4 (cores GC12B, GC13A, GC13B, GC15A; Figs. 9, 10) in the farthest offshore cores within the paleo-Chao Phraya River valley (Fig. 3).

In low diversity (26 taxa) F3, *Heterolepa dutemplei* (13.1%), *Asterorotalia millettii* (11.7%), *Textularia* sp. A (9.4%) and *Hanzawaia nipponica* (7.3%) are the most abundant species (Table 6). F3 clusters closer to F1A, B, C than to F2A and F2B (Fig. 11). This cluster group occurs in Unit 4 and Unit 5 in cores GC9A and GC10A (Figs. 8, 9) from the inner shelf region (Fig. 3).

5. Discussion

5.1. Sedimentologic and foraminiferal characteristics of chronostratigraphic units

The five chronostratigraphic units described above demonstrate lateral and vertical variations in facies and boundaries that provide the foundation for placing them into a sequence stratigraphic framework (Figs. 3, 12, 13). Sediments from two base-level cycles were recovered; the earlier one represents a portion of the late Pleistocene cycle (pre-LGM lowstand), the younger represents the present base-level cycle (post-LGM lowstand), although we did not recover the basal unconformity and early post-LGM fill.

Unit 1 is part of the late Pleistocene base-level cycle, occurs only in one core (GC8A; Figs. 3, 4), and extends to the sediment-water interface. Radiocarbon ages Table 4; Figs. 4, 12) suggest that it was deposited during MIS 3 (although the finite age is very near the limit of the radiocarbon technique). This unit has similar characteristics to the Holocene units found laterally. The elevation of Unit 1 indicates the area surrounding core GC8A is likely a paleo-interfluve between the paleo-Marang valley and the paleo-Chao Phraya valley (Figs. 1B, 3). BMS and elemental data show no significant trends although percent planktonic foraminifera increase upward (Fig. 4), indicating a deepening upwards trend. The geochronology of this core and abundance of planktonic foraminifera (maximum of 8.5%; Table 5) suggest an open marine, inner shelf depositional environment at water depths of ~40–60 m (Table 3). *Asterorotalia pulchella*, *Hanzawaia nipponica* and *Heterolepa dutemplei* are the most abundant benthic foraminifera in GC8A (Fig. 4) similar to core samples from beneath 50 cm core depth (Unit 4) in GC11B (Fig. 7). This indicates that late-Pleistocene depositional environments of Unit 1 were similar to the deepening-upward, open inner shelf, transgressive environment of the late Holocene (cluster group F1C; Fig. 7; Table 6). A sequence boundary (either subaerial unconformity or ravinement surface) corresponding to the LGM is inferred (but not recovered in the cores), separating Unit 1 from the overlying Unit 2, based on the ages that indicate Unit 2 is part of the present base-level cycle (Fig. 12). Based upon the RSL curve (Fig. 2) of Hanebuth et al. (2011), the shelf at core GC8A (current water depth of ca. −60 m would have been subaerially exposed until ca. 12,000 cal yr BP (Figs. 2, 3, 13).

Unit 2 was only recovered in core GC16B on the flank of the paleo-Chao Phraya River valley (Figs. 3, 5, 12) and may occur below our depth of recovery within the incised valley. With an age of ca. 12,700 cal yr BP, Unit 2 is late Pleistocene in age (Younger Dryas) and was deposited during the post-LGM relative sea-level rise. From the bottom

Table 4
AMS Radiocarbon age estimates with associated data and values used in calibration.

Sample ID	Reported ages	Cal. years bp	Midrange cal. yr bp	% age certainty	d13c	δ r	δ r uncertainty	Type
GC1, 146–148	10,400	11,876–11,271	11,570 ± 303	95.4	−28.41	−45	49	Wood
GC3, 24–26	1410	1142–901	1020 ± 121	95.4	−0.31	−45	49	Foraminifera
GC3, 50–52	2350	2175–1871	2020 ± 152	95.4	−0.12	−45	49	Foraminifera
GC3, 100–102	3970	4201–3867	4030 ± 167	95.4	−0.15	−45	49	Foraminifera
GC4, 50–52	635	466–228	347 ± 238	95.4	0	−45	49	Foraminifera
GC4, 100–102	2320	2135–1855	2000 ± 140	95.4	−0.27	−45	49	Foraminifera
GC4, 150–152	4780	5286–4937	5110 ± 175	95.4	−0.4	−45	49	Foraminifera
GC4, 200–202	5530	6166–5837	6000 ± 165	95.4	−0.65	−45	49	Foraminifera
GC5, 28–29	2100	1866–1590	1730 ± 138	95.4	−0.25	−45	49	Foraminifera
GC5, 64–65	4140	4413–4099	4260 ± 157	95.4	NA	−45	49	Foraminifera
GC5, 86–87	4840	5342–4986	5160 ± 178	95.4	−0.29	−45	49	Foraminifera
GC5, 114–115	6020	6633–6347	6490 ± 143	95.4	−0.65	−45	49	Foraminifera
GC5, 168–169	7810	8434–8171	8300 ± 132	95.4	−0.81	−45	49	Foraminifera
GC7, 60–61	5800	6396–6148	6270 ± 124	95.4	−0.7	−45	49	Foraminifera
GC7, 110–111	6220	6872–6571	6720 ± 151	95.4	−0.69	−45	49	Foraminifera
GC7, 154–155	8930	9855–9500	9680 ± 178	95.4	−0.48	−45	49	Foraminifera
GC8A, 62–63	40,700	45,085–42,851	43,970 ± 1117	95.4	−0.82	−45	49	Foraminifera
GC8A, 164–165	45,600	[50,000]–46,711	46,700 ±	95.4	NA	−45	49	Foraminifera
GC9A, 44–45	1680	1381–1171	1280 ± 105	95.4	−0.3	−45	49	Foraminifera
GC9A, 92–93	3290	3346–3009	3180 ± 169	95.4	−0.14	−45	49	Foraminifera
GC9A, 132–133	6580	7263–6999	7130 ± 132	95.4	NA	−45	49	Foraminifera
GC10A, 46–48	3850	4024–3703	3860 ± 161	95.4	−0.53	−45	49	Foraminifera
GC10A, 85–86	6290	6938–6659	6800 ± 140	95.4	−0.51	−45	49	Foraminifera
GC10A, 180–181	7790	8393–8177	8290 ± 108	95.4	NA	−45	49	Foraminifera
GC11B, 46–47	5490	6086–5756	5920 ± 165	95.4	−0.23	−45	49	Foraminifera
GC11B, 113–114	9730	10,892–10,534	10,700 ± 179	95.4	NA	−45	49	Foraminifera
GC16B, 49–50	5040	5562–5313	5440 ± 125	95.4	NA	−45	49	Foraminifera
GC16B, 167–168	11,150	12,814–12,577	12,700 ± 119	95.4	−7.88	−45	49	Mollusc
GC12B, 59–60	3440	3501–3218	3360 ± 142	95.4	−0.38	−45	49	Foraminifera
GC12B, 174–175	8200	8960–8597	8780 ± 182	95.4	−0.7	−45	49	Foraminifera
GC13A, 48–49	5530	6143–5855	6000 ± 144	95.4	−0.24	−45	49	Foraminifera
GC13A, 189–190	8270	9014–8664	8840 ± 175	95.4	−0.71	−45	49	Foraminifera
GC13B, 70–71	4440	4812–4522	4670 ± 145	95.4	−0.38	−45	49	Foraminifera
GC13B, 188–189	7250	7888–7643	7770 ± 123	95.4	NA	−45	49	Foraminifera
GC14B, 35–36	3750	3880–3590	3740 ± 145	95.4	−0.04	−45	49	Foraminifera
GC14B, 70–71	10,150	11,332–11,051	11,190 ± 141	95.4	−11.39	−45	49	Mollusc
GC15A, 39–41	1530	1254–1005	1130 ± 125	95.4	−0.32	−45	49	Foraminifera
GC15A, 118–119	5550	6145–5884	6010 ± 131	95.4	NA	−45	49	Foraminifera
GC15A, 219–221	8780	9600–9380	9490 ± 110	95.4	−1.11	−45	49	Foraminifera

of the unit in core GC16B to ca. 110 cm, the cosmopolitan shallow water species *Ammonia tepida* strongly dominates the benthic assemblage (Fig. 5). The absence of planktonic foraminifera and the low diversity cluster group F1A suggest a shallow nearshore setting. *Ammonia tepida* is also characteristic of brackish bays and estuaries (e.g., Sen Gupta, 1999; McGann et al., 2013). Given the age estimate (12,700 ± 119 cal yr BP) from 167 to 168 cm in core GC16B, the present elevation of the unit (ca. −72 to −73 m), and the position of RSL at that time (ca. −65 m; Hanebuth et al., 2011; Fig. 2), sediments of Unit 2 were deposited in water depths of ca. 10 m or less. The age, elevation, and foraminiferal composition suggest that this unit is part of the post-LGM transgressive systems tract (Figs. 3, 13).

Unit 3 shows a significant lateral variation in depositional environment along a depth gradient during the earliest Holocene. The sediments are only slightly (ca. 1000–1500 years) younger than the sediments of Unit 2. However, rapid RSL rise during this time began the submergence of the shelf west of the paleo-Chao Phraya River valley. During deposition of Unit 3 (ca. 11,570–11,190 cal yr BP; Fig. 12) relative sea-level on the Sunda Shelf was approximately −60 to −50 m (Hanebuth et al., 2011; Fig. 2). Given the present elevation of the black, organic-rich mud facies (Fig. 7) in GC14B (ca. −69 m), this part of the unit was deposited at a water depth of ca. 15 m. Foraminiferal assemblages in the organic-rich mud are dominated by shallow shelf species *Asterorotalia pulchella*, *Textularia haueri*, and *Assilina ammonoides* and show relatively low numbers of species and calculated number of tests/g sediment (GC14B; Fig. 7; Table 5), consistent with a shallow inner shelf environment. The cluster group (F1B) of this facies is most closely associated with cluster group F1C (Fig. 11) from GC11B on the inner shelf (Fig. 3), suggesting similar depositional environments in these two areas. The peaty mud facies (barren of foraminifera) occurs shallower, (ca. −52 m in GC1 and − 55 m in GC2; Figs. 3, 6). Modern mangrove swamp sediments of the east coast of peninsular Malaysia are characterized by delicate agglutinated foraminifera with a low preservation potential over timescales of thousands of years (Culver et al., 2013, 2015). Nevertheless, these peaty mud deposits likely represent deposition just below sea level in a coastal wetland similar to the extensive mangrove wetlands in the region today.

Unit 3 is bounded at the top by an erosional surface (an irregular contact with greater sand content and shell layers) overlain in core GC14B by grey shell-rich sandy muds containing planktonic foraminifera; i.e., a deeper water facies (Fig. 7; Table 5). The characteristics of the boundary (coarser sediments than below or above, and with a shell lag) suggest elevated energy conditions. Thus, the erosional discontinuity may represent a ravinement surface (either wave or tidal) related to increased inundation of the shelf, greater fetch, and greater exposure to swell, as well as an increase in tidal currents (although we see no evidence of tidal bedding). The age of this surface (ca. 11,200 cal y BP) is consistent with the age of the TRS on the central Sunda Shelf as described by Hanebuth and Stattegger (2003) and slightly earlier than

Table 5
Values for foraminiferal characteristics by sample (10 cores).

Sample ID, sample depth	No. specimens picked	no. species (S)	Calc. no. tests/1 g	Fisher's alpha	% planktonics	% textulariid	% miliolid	% rotaliid
GC9A 23–24	283	40	230	12.7	1.77	24.03	7.07	67.14
GC9A 35–36	297	37	183	11.1	4.04	27.61	4.38	63.97
GC9A 47–48	290	33	131	9.6	4.14	31.03	8.28	56.56
GC9A 59–60	303	36	67	10.6	2.97	23.1	4.95	68.98
GC9A 71–72	300	35	76	10.2	3.67	25.67	6.33	64.33
GC9A 83–84	290	35	136	10.4	6.21	31.38	6.55	55.86
GC9A 95–96	312	35	2053	10.1	3.21	38.46	8.97	49.36
GC9A 107–108	319	32	580	8.8	2.51	40.75	7.52	49.22
GC9A 119–120	304	37	157	11.1	0.99	37.83	15.13	46.05
GC9A 131–132	280	35	142	10.5	1.07	34.64	18.93	45.36
GC9A 143–142	294	48	74	16.1	0.68	25.85	25.51	47.96
GC10A 34–35	299	29	197	7.9	1.33	29.77	5.02	63.88
GC10A 46–47	313	35	58	10.1	3.19	30.67	6.07	60.06
GC10A 58–59	286	33	179	9.5	1.05	33.57	7.69	57.69
GC10A 70–71	272	33	394	9.8	2.21	45.59	9.93	42.28
GC10A 82–83	320	28	1833	7.4	0.63	47.19	6.88	45.31
GC10A 94–95	290	29	106	8	0.69	44.14	4.83	50.34
GC10A 106–107	314	39	33	11.8	2.87	23.89	14.64	58.6
GC10A 118–119	302	36	23	10.6	2.98	28.81	12.91	55.3
GC10A 130–131	250	34	22	10.6	4.4	13.6	27.2	54.8
GC10A 142–143	274	43	16	14.4	1.09	30.29	15.69	52.92
GC10A 154–155	147	36	10	15	2.04	25.85	19.05	53.06
GC10A 166–167	288	41	20	13	2.43	21.18	25.69	50.69
GC10A 178–179	225	38	21	13	0.44	36.44	17.78	45.33
GC10A 190–191	255	39	32	12.7	0.78	33.73	19.22	46.27
GC11B 37–38	323	43	226	13.7	1.27	16.35	10.9	72.76
GC11B 46–47	307	37	268	10.9	1.3	19.8	10.56	69.94
GC11B 61–62	311	33	70	9.4	0	7.57	11.51	80.92
GC11B 70–71	308	29	31	7.8	0	8.17	9.15	82.68
GC11B 82–83	304	34	92	9.8	0.32	16.94	14.01	69.06
GC11B 94–95	222	23	29	6.5	0	15.14	10.09	74.77
GC11B 104–105	140	16	17	4.6	0	23.08	5.59	71.33
GC11B 118–119	304	30	19	5.3	0	12.75	8.5	78.76
GC8A 17–18	267	46	38	15.9	8.5	12.5	11.07	76.43
GC8A 32–33	288	34	14	9.9	1.26	9.87	2.23	87.9
GC8A 44–45	284	45	23	15.1	4.87	5.46	2.73	91.81
GC8A 56–57	187	29	9	9.5	0	8.06	5.91	86.02
GC8A 68–69	265	37	12	11.6	1.97	6.02	6.35	87.63
GC8A 80–81	279	35	12	10.5	2.99	4.11	8.56	87.33
GC8A 92–93	304	46	21	15.1	0.98	9.6	12.91	77.48
GC8A 104–105	289	40	26	15.6	0.65	9.54	11.84	78.62
GC8A 116–117	303	39	21	11.9	0.98	7.89	12.83	79.28
GC8A 128–129	315	43	60	13.4	0.31	8.52	11.99	79.5
GC8A 140–141	323	38	56	11.2	0	6.91	7.51	85.59
GC8A 152–153	319	43	99	13.4	0.31	14.47	10.69	74.84
GC8A 164–165	309	41	109	12.7	0.32	13.03	8.47	78.5
GC15A 26–27	248	41	175	13.9	23.39	15.73	12.5	48.39
GC15A 45–46	312	49	2013	16.4	25	11.86	16.35	46.79
GC15A 65–66	269	47	2690	16.4	13.01	17.84	16.36	52.79
GC15A 85–86	318	55	4818	19.1	16.67	23.9	19.18	40.25
GC15A 105–106	262	37	32,750	11.8	11.83	26.34	14.5	47.33
GC15A 125–126	315	43	2864	13.4	10.16	34.92	15.56	39.37
GC15A 145–146	272	40	1537	13	3.68	28.68	26.1	41.54
GC15A 165–166	304	38	1143	11.5	4.28	30.26	18.42	47.04
GC15A 185–186	260	43	1677	14.7	1.92	38.08	20	40
GC15A 205–206	282	48	605	16.7	1.42	28.37	21.99	48.23
GC15A 221–222	203	39	832	14.5	1.48	23.65	24.14	50.74
GC14B 26–27	316	42	1090	13	14.24	14.24	13.92	57.59
GC14B 45–46	220	50	2650	20.2	12.27	17.73	10	60
GC14B 65–66	200	37	8	13.4	7.5	22.5	10	60
GC14B 85–86	59	20	2	10.5	3.39	10.17	6.78	79.66
GC14B 105–106	55	20	4	11.3	7.27	16.36	1.82	74.55
GC14B 125–126	71	26	3	15	14.08	4.23	12.68	69.01
GC14B 134–135	136	29	5	11.3	0.74	16.18	8.09	75
GC13B 36–37	285	49	95,335	17.1	14.39	27.37	14.39	43.86
GC13B 55–56	324	45	38,896	14.3	12.04	37.65	9.26	41.05
GC13B 75–76	247	46	1594	16.6	5.67	25.91	20.24	48.18
GC13B 95–96	225	49	1621	19.3	6.67	16.44	20.44	56.44
GC13B 115–116	291	48	936	16.4	2.41	25.43	27.15	45.02
GC13B 135–136	252	45	1335	16	2.38	24.21	23.41	50
GC13B 155–156	287	50	923	17.6	1.74	29.27	17.77	51.22
GC13B 175–176	287	44	1852	14.5	4.53	25.09	20.91	49.48
GC13B 189–190	249	43	2360	15	2.41	23.69	18.88	55.02
GC13A 43–44	288	45	8727	15	10.07	31.25	14.24	44.44

(*continued on next page*)

Table 5 (*continued*)

Sample ID, sample depth	No. specimens picked	no. species (S)	Calc. no. tests/1 g	Fisher's alpha	% planktonics	% textulariid	% miliolid	% rotaliid
GC13A 63–64	262	48	3403	17.3	12.21	29.39	16.41	41.98
GC13A 83–84	276	46	8364	15.8	7.97	30.43	14.49	47.1
GC13A 103–104	262	54	3970	20.7	14.89	23.28	23.28	38.55
GC13A 123–124	279	51	1800	18.3	9.32	20.43	30.11	40.14
GC13A 143–144	266	51	855	18.7	6.02	29.32	21.43	43.23
GC13A 163–164	270	46	8182	15.9	8.15	27.04	19.26	45.56
GC13A 183–184	339	57	1389	19.6	4.42	18.88	23.6	53.1
GC13A 192–193	236	40	1180	13.4	3.81	28.81	16.1	51.27
GC12B 48–49	274	37	16,506	11.5	12.77	29.2	7.66	50.36
GC12B 67–68	258	37	15,542	11.8	12.02	32.17	14.34	41.47
GC12B 87–88	258	38	3909	12.3	15.5	35.66	14.73	34.11
GC12B 107–108	251	43	4564	15	18.33	33.47	19.52	28.69
GC12B 127–128	287	44	17,289	14.4	16.72	27.87	13.94	41.46
GC12B 147–148	268	51	10,141	18.6	16.04	20.52	17.16	46.27
GC12B 167–168	274	42	881	13.8	4.01	20.44	24.09	51.46
GC12B 181–182	184	31	1187	10.7	5.98	28.8	20.11	45.11
GC16B 46–47	257	38	11,682	12.3	8.56	30.35	9.34	51.75
GC16B 65–66	300	49	9090	16.6	6.33	33	12	48.67
GC16B 85–86	62	20	3	10.5	11.29	19.35	4.84	64.52
GC16B 105–106	37	16	1	NA	10.81	18.92	0	70.27
GC16B 125–126	29	7	1	NA	0	17.24	0	82.76
GC16B 145–146	12	2	0.03	NA	0	8.33	0	91.67
GC16B 165–166	30	1	2	NA	0	0	0	100
GC16B 185–186	130	4	4	0.8	0	0	0	100
GC16B 205–206	2	2	0.05	NA	0	0	50	50
GC16B 213–214	211	37	6	13	5.69	50.71	9.95	33.65

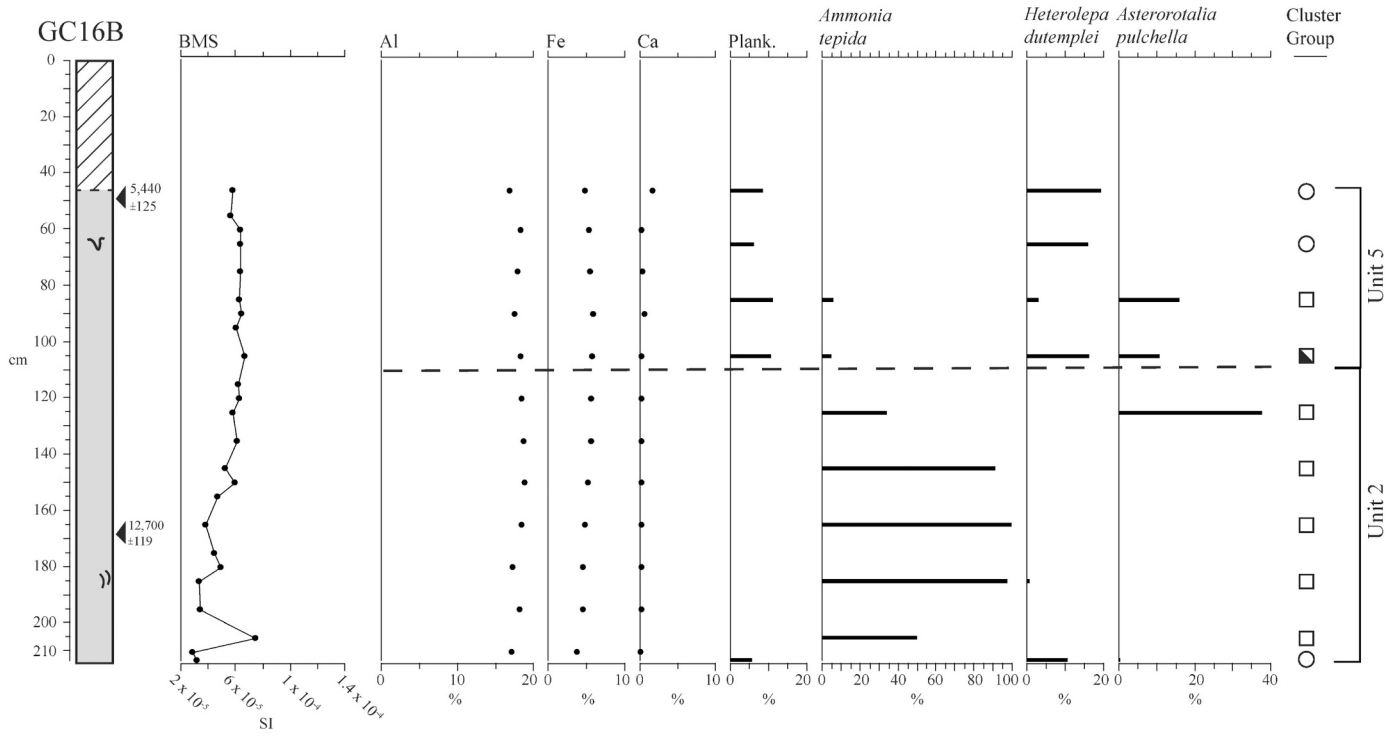

Fig. 5. Lithologic log for core GC16B (71 m water depth), composed of chronostratigraphic Units 2 and 5, with calibrated radiocarbon age estimates, BMS, Al, Fe, and Ca plots, percent planktonic foraminifera, relative abundance of the three most abundant benthic foraminiferal species, and foraminiferal cluster group membership (see Fig. 11). The lowermost sample is contaminated with modern sediment due to core bounce on recovery. See Fig. 4 for key to core log symbols.

ravinement described by Puchala et al. (2006) at 10,400 cal y BP in the central Gulf of Thailand. The BMS and elemental profiles in Unit 3 of core GC14B are relatively uniform beneath the discontinuity (Fig. 7), but display an abrupt increase in BMS and percent Ca, and decreases in percent Al and Fe across the erosional contact (Fig. 7). This suggests a decreased terrestrial sediment influence as Al and Fe are associated with the products of terrestrial weathering (clays, Fe-oxides) (Wehausen and Brumsack, 2002; Bahr et al., 2005), again consistent with a deeper water facies above the boundary. Based on these data, we interpret Unit 3 as a coastal (in the west) to inner shelf unit belonging to the transgressive systems tract (Figs. 3, 13).

Unit 4 occurs on the inner shelf at an elevation of approximately −57

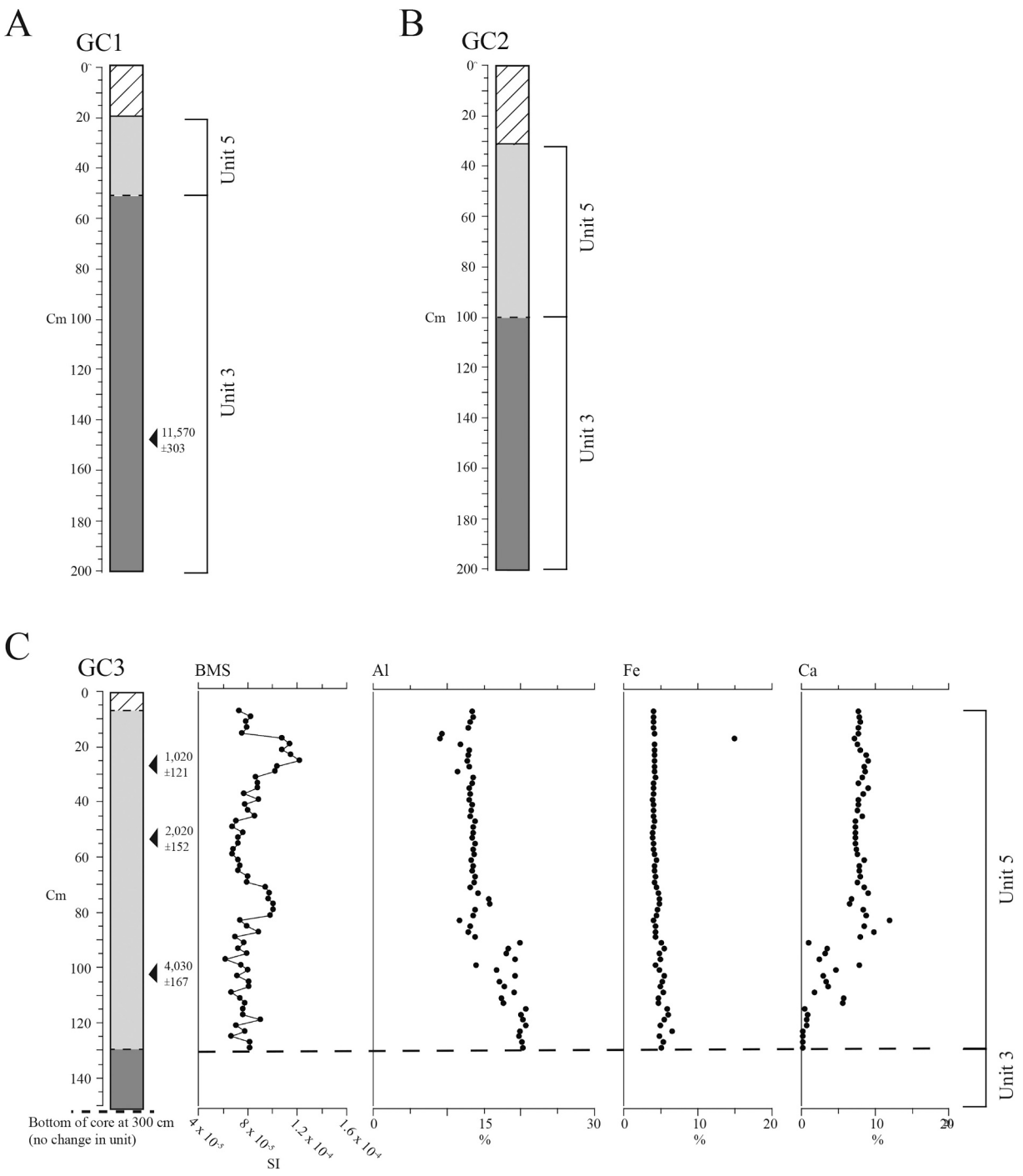

Fig. 6. Lithologic logs and associated data: A: core GC1 (51.5 m water depth), composed of chronostratigraphic Units 3 and 5, with calibrated radiocarbon age estimate; B: core GC2 (53.6 m water depth), composed of chronostratigraphic Units 3 and 5; C: core GC3 (54.9 m water depth), composed of chronostratigraphic Units 3 and 5, with calibrated radiocarbon age estimates, and BMS, Al, Fe, and Ca plots. See Fig. 4 for key to core log symbols.

to −59 m, and farther seaward within the paleo-Chao Phraya valley at an elevation of approximately −72 to −78 m (Fig. 3). Note that we did not recover the base of Unit 4 within the paleo-Chao Phraya River valley, so its true thickness there is not known. Interpreted in the context of regional sea-level curves, the age estimates (ca. 10,900–6350 cal yr BP; Fig. 12) indicate deposition in increasing water depth ranging from ca. 10 m (for the oldest sediments) to ca. 60 m (for the youngest sediments). The upper portion of the unit corresponds approximately to the ca. 6500 cal yr BP highstand on the shelf (Fig. 2). The lower section exhibits significant terrestrial influence as indicated by greater values of BMS and greater percent Al and Fe (Table 3; Figs. 8–10), in agreement with the interpretation of a shallow, nearshore environment based on the relative sea-level curve. The upward decrease in Al and Fe values, and increase in Ca values, suggest an increase in marine biogenic carbonate

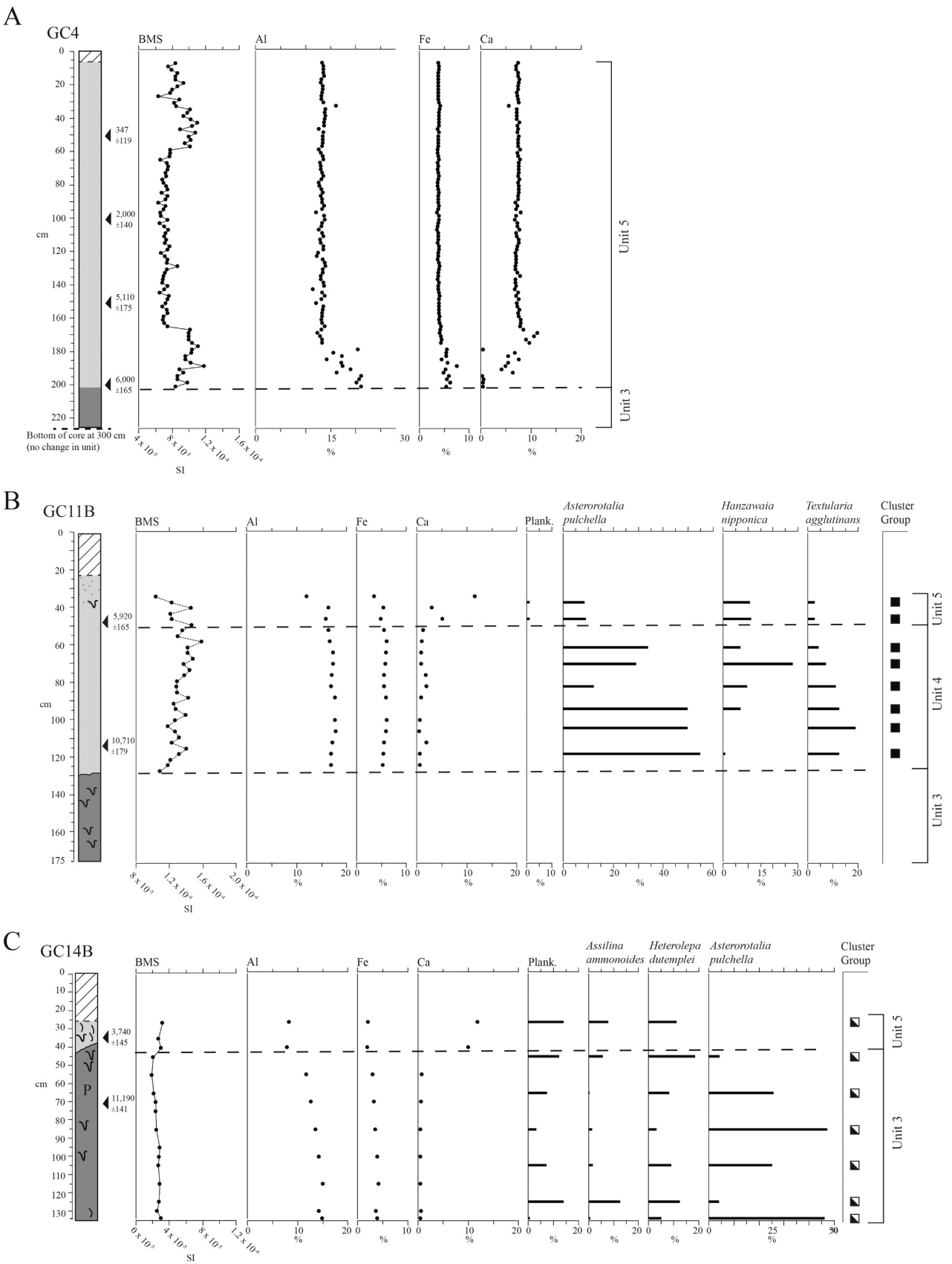

Fig. 7. Lithologic logs. A: core GC4 (56 m water depth), composed of chronostratigraphic Units 3 and 5; B: core GC11B (57.2 m water depth), composed of chronostratigraphic Units 3, 4 and 5; C: core GC14B (68 m water depth), composed of chronostratigraphic Units 3 and 5; with calibrated radiocarbon age estimates, BMS, Al, Fe, and Ca plots, percent planktonic foraminifera, relative abundance of the three most abundant benthic foraminiferal species, and foraminiferal cluster group membership (see Fig. 11). See Fig. 4 for key to core log symbols.

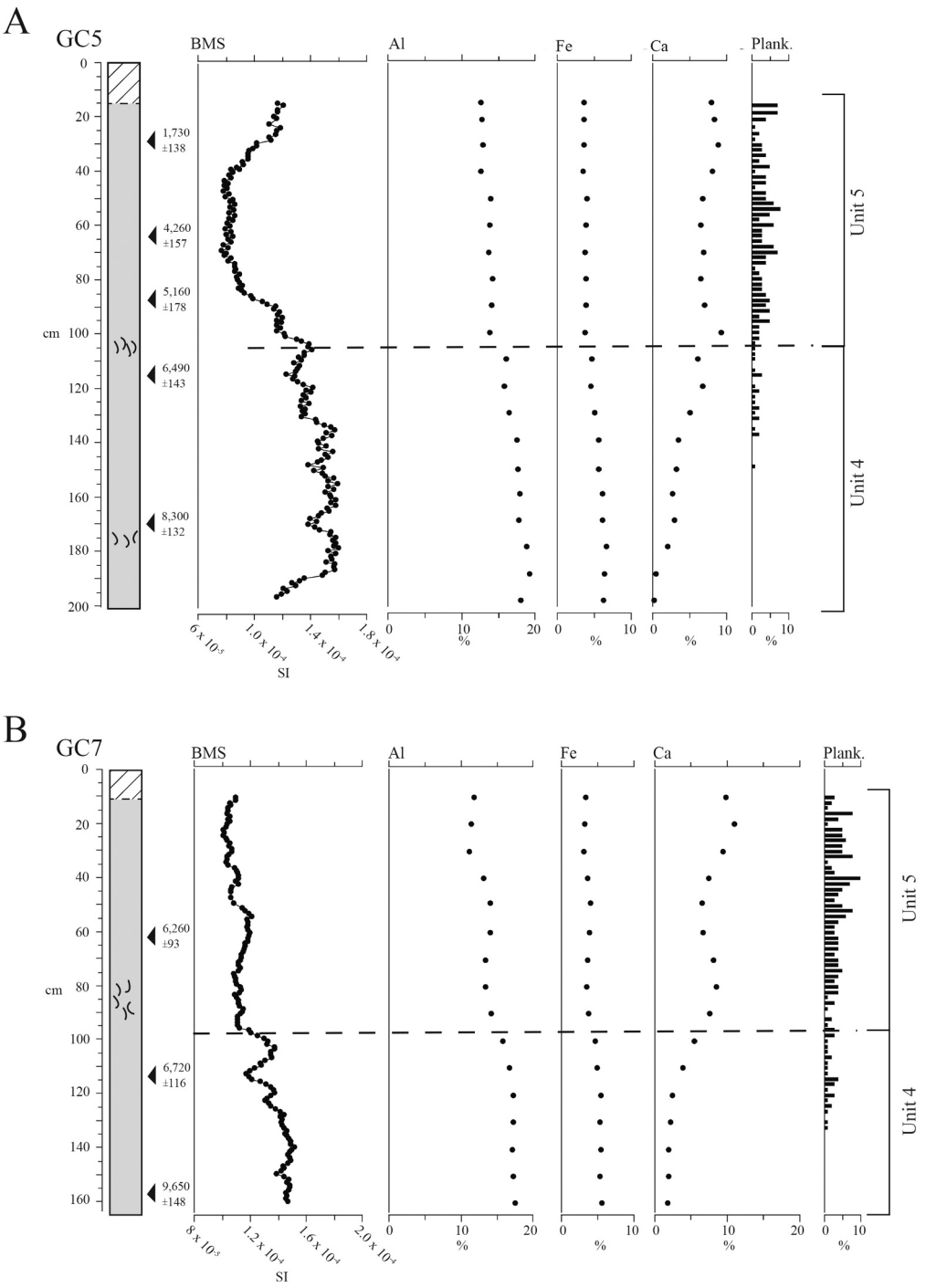

Fig. 8. Lithologic logs. A: core GC5 (58 m water depth), composed of chronostratigraphic Units 4 and 5; B: core GC7 (59 m water depth), composed of chrostratigraphic Units 4 and 5; C: core GC9A (56.5 m water depth), composed of chronostratigraphic Units 4 and 5; with calibrated radiocarbon age estimates, BMS, Al, Fe, and Ca plots, percent planktonic foraminifera, relative abundance of the three most abundant benthic foraminiferal species, and foraminiferal cluster group membership (see Fig. 11). See Fig. 4 for key to core log symbols.

and decrease in terrestrial sediments, also suggesting a rising sea level and increasing distance from terrestrial sources. Based on these data, we interpret Unit 4 as a deepening-upward open inner shelf unit also belonging to the transgressive systems tract (Figs. 3, 13).

Cluster analysis of foraminiferal data from Unit 4 show significant cross-shelf changes. Data from inner shelf cores GC10A and GC9A, within the paleo-Marang and paleo-Terengganu river valleys group into the low diversity F3 (Fig. 11). The slightly more seaward core, CG11B, is characterized by the higher diversity F1C (Fig. 7). Within paleo-Chao Phraya valley cores (GC12B, GC13A, GC13B, and GC15A), Unit 4 samples cluster into the high diversity group F2B (Table 6; Fig. 11). Thus, a clear trend of increasing diversity takes place in a seaward direction.

Unit 5 drapes the shelf, is thickest (2 m) in core GC4 (Fig. 7), and thins landward and seaward (Fig. 3). It pinches out between GC7 and GC8, near the 60 m isobath, then occurs again within the paleo-Chao Phraya River valley below the 70 m isobath, and thins to a feather

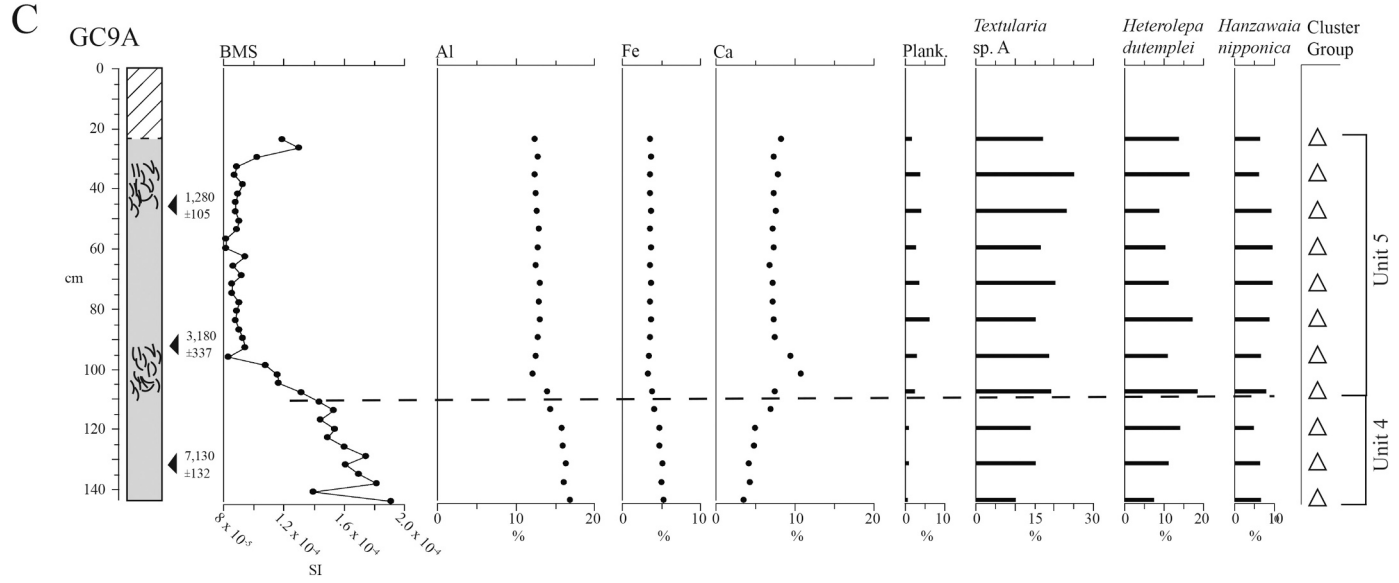

Fig. 8. (*continued*).

edge at GC14B (Figs. 3, 7). This unit is characterized by ages that are less than ca. 6500 cal yr BP (Fig. 12), and by major changes in the foraminiferal assemblages (Table 5) relative to underlying units in the paleo-Chao Phraya valley. Foraminiferal changes include the presence of significantly more planktonic foraminifera, increase in calculated number of specimens per gram of sediment, replacement of the shallow-water *Ammonia tepida* by *Heterolepa dutemplei,* and increase in species diversity (richness, S and Fisher's alpha). Percent planktonic foraminifera and percent *Heterolepa dutemplei* increase with both distance from shore and water depth in this region (Martin et al., 2018), indicating a more offshore depositional environment for Unit 5 than underlying units.

Cluster groups of Unit 5 are similar to those in the underlying Unit 4. Inner shelf cores show the low diversity F3 cluster group, whereas the more offshore cores within the paleo-Chao Phraya River valley cluster into the high diversity group F2A (Fig. 11). Cluster groups F2B (in Unit 4) and F2A (in Unit 5) are overall quite similar (Fig. 11), with similar diversity (Table 5), and in both *Heterolepa dutemplei* is the most abundant species (Table 5). They are distinguished in the cluster analysis by the codominance of *Textularia* sp. A in Unit 5 (F2A) whereas F2B in Unit 4 shows less dominance (Table 6).

Unit 5 exhibits overall lower BMS (7.63×10^{-5} SI), Al (13.6 wt%), Fe (3.7 wt%), and higher Ca (7.33 wt%) than Unit 4, which suggests deeper water conditions and a more distal setting relative to the shoreline (Table 3; Fig. 3). These characteristics, and the significantly increased water depth that is indicated, based on the comparison of regional RSL curves (Fig. 2) and geochronology, indicate that the change occurred ~6500 cal yr BP and is marked in cores GC5, GC15A, GC7, GC9A, GC10A (Figs. 8–10) by a burrowed shelly mud along the boundary between Unit 4 and Unit 5. This boundary is interpreted as the maximum flooding surface (MFS) (Figs. 3, 13) and Unit 5 represents the HST. Radiocarbon age estimates (6610 ± 131 cal yr BP to 1130 ± 125 cal yr BP) (Figs. 12, 13), and comparison to the RSL curve (Fig. 2) indicate deposition in generally stable water depths similar to, or 2–4 m higher (deeper), than today (highstand on the Sunda Shelf ca. 6500 cal yr BP; Hanebuth et al., 2011; Mallinson et al., 2014; Parham et al., 2014;).

During the transition from Unit 4 to Unit 5, the shoreline had transgressed to its maximum landward extent by ca. 7000 cal yr BP (Parham et al., 2014). At this time the shoreline along the east coast of Peninsular Malaysia was approximately 2–10 km inland of its present location (Mallinson et al., 2014; Parham et al., 2014), and the shelf experienced lower terrestrial sediment input. In situ fossil corals occur at an elevation of +1.3 m 20 km north of Kuala Terengganu, buried beneath beach ridge sands, and were dated to 7200–6900 cal yr BP (Parham et al., 2014). Since then, the coastal system has built seaward, driven by sedimentation and the relative sea-level fall with short term minor oscillations related to ENSO and monsoon conditions, and the influx of sediments that constructed strandplains and barrier islands (during intervals of rising relative sea-level; Mallinson et al., 2014).

5.2. Regional summary and environmental evolution

The sequence stratigraphic framework presented above is recognized on the basis of the diverse data set acquired from the core samples. The units illustrate the progressive change in depositional environments upward and cross-shelf during the most recent base-level rise, beginning with the subaerial unconformity of the LGM. The LGM lowstand of ca. 120 m below modern sea level (Fairbanks, 1989) was low enough to expose the entire Sunda Shelf (Voris, 2000; Sathiamurthy and Voris, 2006) and resulted in incised valley systems (Hanebuth and Stattegger, 2003). Although there are detailed seismic surveys of several segments of Sunda Shelf paleovalleys (Miall, 2002; Darmadi et al., 2007; Reijenstein et al., 2011; Puchala et al., 2011; Alqahtani et al., 2015; Rahman et al., 2016), published core data on the Shelf are very limited (in terms of number and distribution) (Hanebuth and Stattegger, 2003; Puchala et al., 2011; Alqahtani et al., 2015, 2017; this study). Geochronologic and biostratigraphic data are also generally lacking. Modern bathymetric data suggest greater lowstand valley incision downstream (40 m of relief in the central submarine valley of the North Sunda River; Hanebuth and Stattegger, 2003), with the potential for considerable post-LGM marine sediment accumulation during sea-level rise and highstand, with incision decreasing upstream in both trunk valleys and tributaries.

The ca. 15–18 m thick Holocene sediment record interpreted to lie within the margins of the paleo-Chao Phraya River incised valley by Alqahtani et al. (2015) was not recovered in this study. Based mainly on

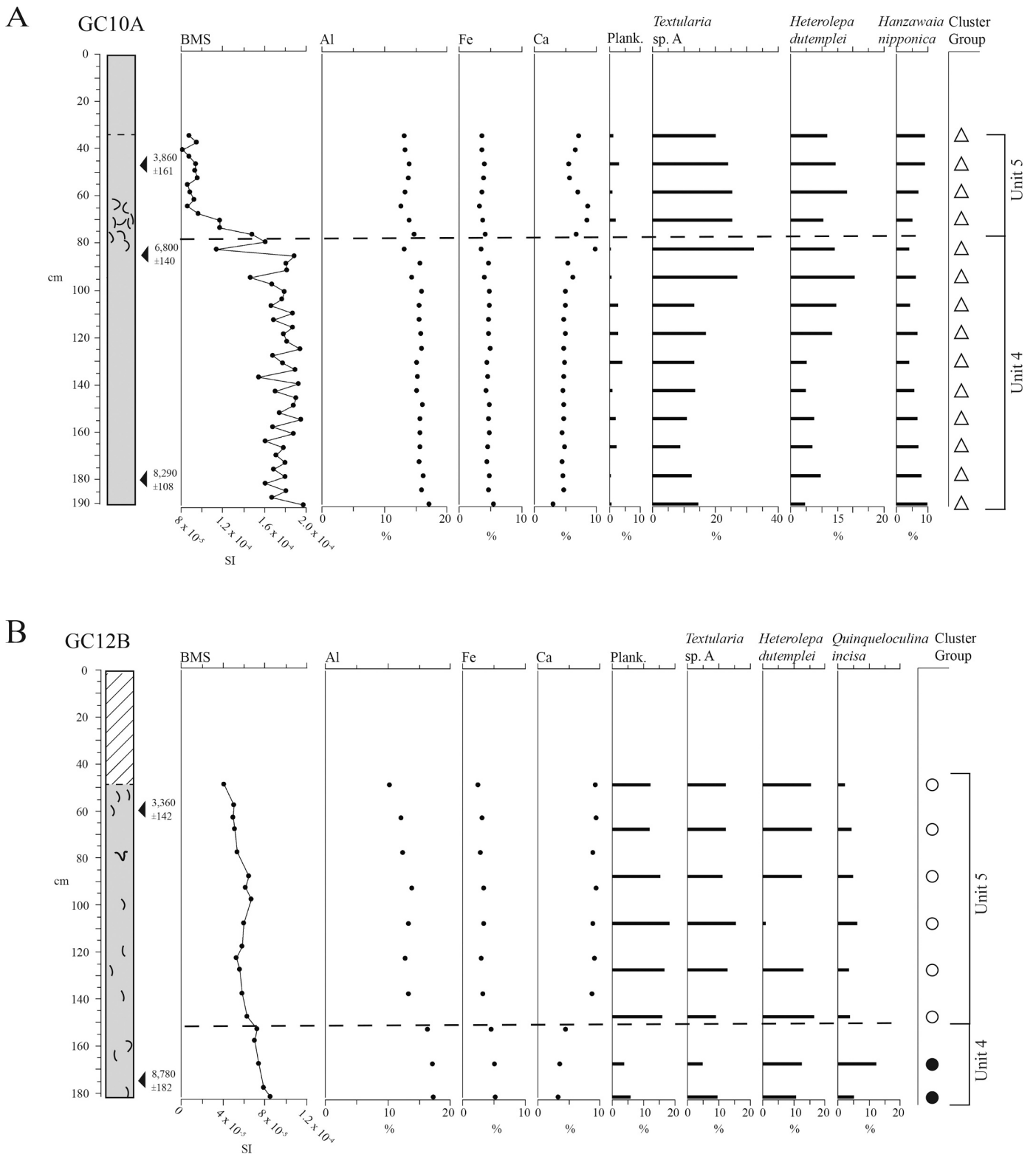

Fig. 9. Lithologic logs.for A: core GC10A (55.7 m water depth), composed of chronostratigraphic Units 4 and 5; B: core GC12B (75 m water depth), composed of chronostratigraphic Units 4 and 5; C: core GC13A (73 m water depth), composed of chronostratigraphic Units 4 and 5; with calibrated radiocarbon age estimates, BMS, Al, Fe, and Ca plots, percent planktonic foraminifera, relative abundance of the three most abundant benthic foraminiferal species, and foraminiferal cluster group membership (see Fig. 11). See Fig. 4 for key to core log symbols.

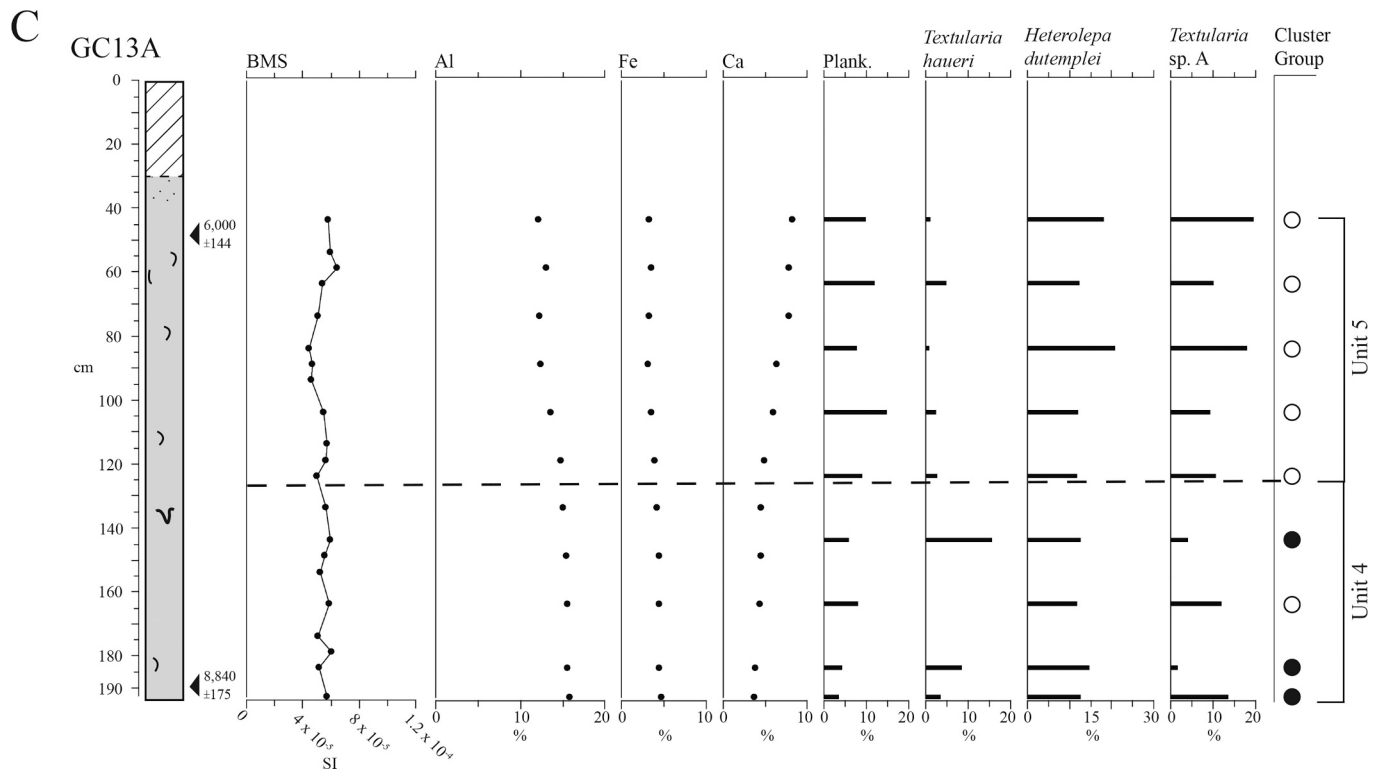

Fig. 9. (*continued*).

geophysical data, several authors have reported 2 m to possibly 29 m of fluvial and marine mud in incised valleys on the Sunda Shelf (Miall, 2002; Darmadi et al., 2007; Reijenstein et al., 2011; Puchala et al., 2011; Rahman et al., 2016). The cores of the current study indicate at least 2 m to a maximum of 3 m (based on calculated accumulation rates from the cores) of Holocene marine sediment accumulation within the margins of the paleo-Chao Phraya River incised valley (Figs. 3, 13). Unpublished geophysical data (Dr. David Menier, personal communication) suggest that the Terengganu and Marang river channels are incised to ca. 20 m below the seafloor. Given that we penetrate to the base of Holocene marine units within two meters, we can assume the lower portions of the valleys are filled with coastal to fluvial sediments. The thin nature of Holocene marine sediments here is similar to that recorded by Hanebuth and Stattegger (2003) and Hanebuth et al. (2011) in the paleo-North Sunda River incised valley. Tjallingii et al. (2010), Puchala et al. (2011) and Rahman et al. (2016) demonstrated that fluvial deposits had almost filled incised valleys on the northern and western Sunda Shelf prior to Holocene marine inundation by post-LGM rising sea level. Rahman et al. (2016) showed that modern bathymetry offshore of the Pahang River (possibly a paleo-tributary of the Siam River; Fig. 1A) does not reflect the location of underlying incised valleys. In contrast, the main valley of the North Sunda River is up to 40 m deeper than the adjacent shelf (Hanebuth and Stattegger, 2003). In the current study area (Malay Basin; Fig. 1A, B), the location of the main paleo-Chao Phraya incised valley, based on geophysical data (Alqahtani et al., 2015), underlies a minor modern seabed low marked by the 70 m bathymetric contour (Figs. 1 and 3).

The stratigraphic record of this study, summarized in Table 3, closely resembles that of the upper units offshore of peninsular Malaysia in the Malacca Strait (Emmel and Curray, 1982), the seismic interpretations of Evans et al. (1995) between Borneo and SE peninsular Malaysia, and the suite of cores within the incised valleys of the paleo-North Sunda River (Hanebuth and Stattegger, 2003), the paleo-Mekong River (Tjallingii et al., 2010) and the paleo-Chao Phraya River and tributaries in the Gulf of Thailand (Puchala et al., 2011; Reijenstein et al., 2011; Sathiamurthy and Rahman, 2017). The late Pleistocene/early Holocene transgressive shallow marine deposits of this study, Units 2 and 3, are equivalent to the Hanebuth and Stattegger (2003) and Hanebuth et al. (2011) transgressive unit. Hanebuth et al. (2011) show the transgressive ravinement surface that we also recognize. Units 4 and 5 of this study are equivalent to the surficial Holocene marine unit of Hanebuth and Stattegger (2003). Unit 4 (TST) transitions across a maximum flooding surface to Unit 5 (HST) ca. 6500 cal yr BP, at the onset of the highstand on the shelf (Table 3). The timing of the maximum flooding surface is consistent with initial progradation of the Chao-Phraya delta to the north beginning at ca. 7000 cal y BP (Tanabe et al., 2003). This last interpretation differs slightly from Hanebuth et al. (2011) in that they show the transition from the transgressive unit to a highstand condensed section at approximately 10 ka. Our placement of the maximum flooding surface at ca. 6500 cal y BP is based on several lines of evidence and is well-constrained, which suggests significant diachroneity of surfaces (TRS and MFS) across the Sunda Shelf related to depth and regional sedimentation patterns.

Although we did not recover the earliest transgressive deposits within the valleys, some comparison to published sequence stratigraphic models of incised valley fill may still be made (Dalrymple et al., 1992; Dalrymple et al., 1994; Zaitlin et al., 1994; Boyd et al., 2006). Given the shallow position of the TRS and MFS, it is clear that high rates of sediment accumulation must be invoked within the valleys during sea-level rise. The Terengganu River occupies a piedmont incised-valley (Boyd et al., 2006), and has a significant suspended sediment load as well as a bedload characterized by coarse, immature sediments. The Marang River occupies a coastal plain incised-valley which yields finer grain sediment as coastal sands are reworked. Regardless, given the very high

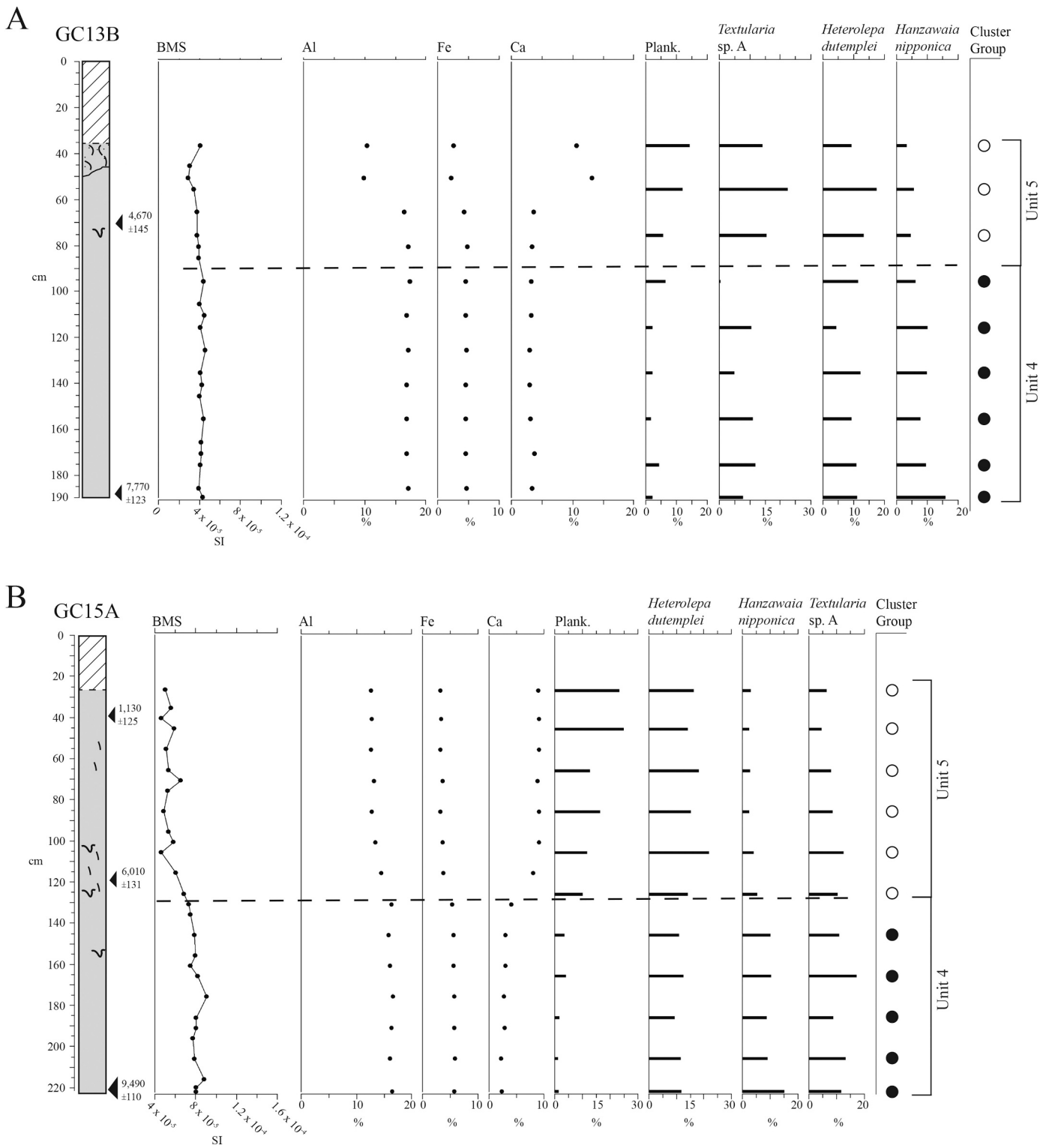

Fig. 10. Lithologic log for: A, core 13B (73 m water depth), composed of chronostratigraphic Units 4 and 5; B, core GC15A (77 m water depth) composed of chronostratigraphic Units 4 and 5; with calibrated radiocarbon age estimates, BMS, Al, Fe, and Ca plots, percent planktonic foraminifera, relative abundance of the three most abundant benthic foraminiferal species, and foraminiferal cluster group membership (see Fig. 11). See Fig. 4 for key to core log symbols.

rates of sediment flux from southeast Asian rivers in general, due to the monsoon precipitation, and a greater drainage area and lower base-level during lower sea-level, it is likely that fluvial sediments are responsible for a significant portion of the paleo-Terengganu and paleo-Marang valley fill, as they are in the modern river channels. This is also supported by the works of Tjallingii et al. (2010), Puchala et al. (2011) and Rahman et al. (2016) who show regional river valleys that are filled with fluvial sediments. Models of Zaitlin et al. (1994) and Boyd et al. (2006) suggest that valleys experiencing high rates of fluvial sediment flux during transgression may be completely filled with fluvial sediments and the transgressive ravinement surface should coincide with the top of the valley fill. Simms et al. (2006) referred to this condition as "overfilled"

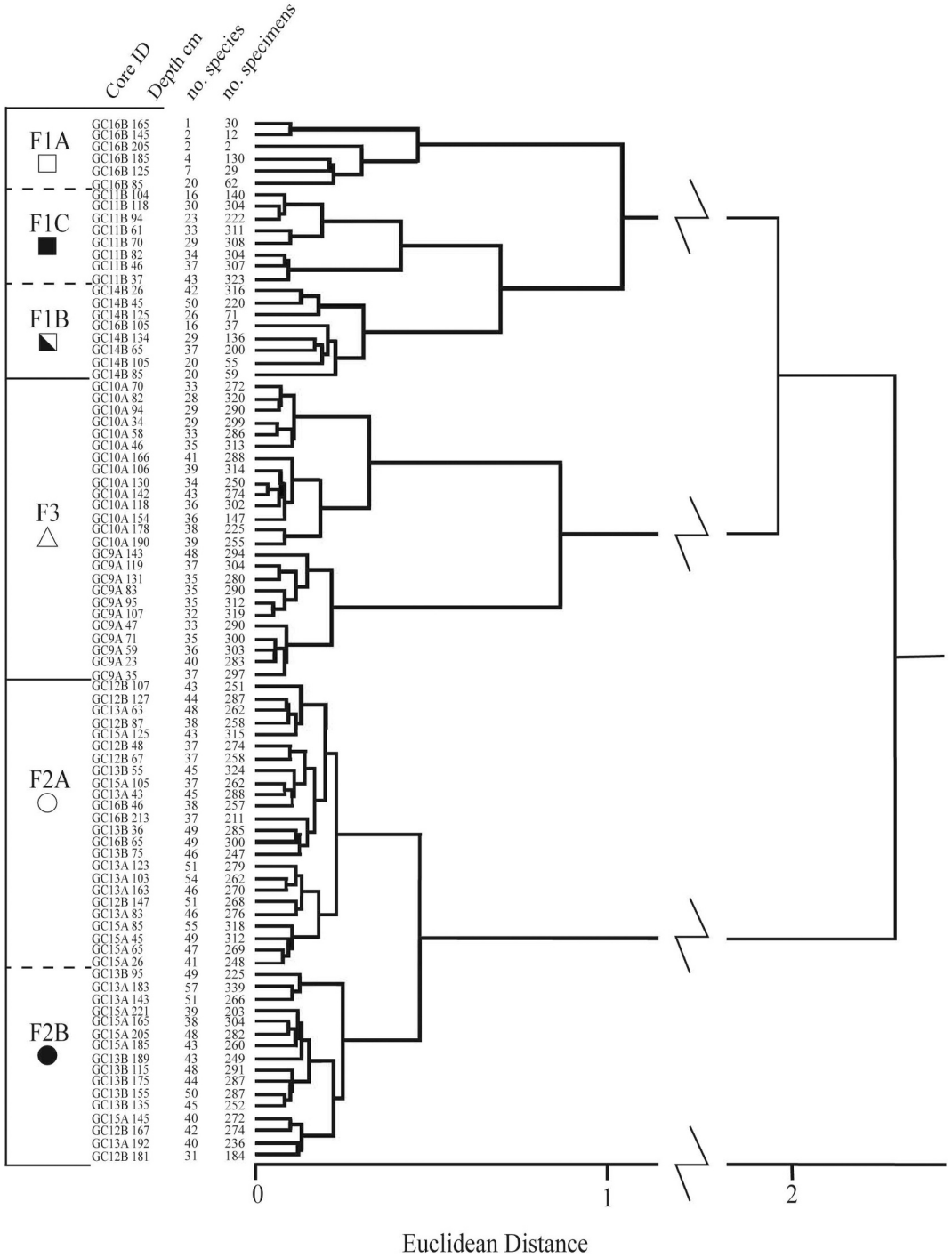

Fig. 11. Dendrogram resulting from cluster analysis of benthic foraminiferal relative abundance data in core samples and showing three major cluster groups, F1, F2, FG3 and subgroups.

Table 6
Composition of benthic foraminiferal assemblages (F1–F3) defined by cluster analysis foraminiferal relative abundance data from all Holocene core samples containing foraminifera.

F1A	Mean	Range	F1B	Mean	Range	F1C	Mean	Range
6 Samples, 18 Taxa	%	%	8 Samples, 53 Taxa	%	%	8 samples, 20 taxa	%	%
Ammonia tepida	63.38	6.45–100.0	*Asterorotalia pulchella*	20.6	0–47.46	*Asterorotalia pulchella*	30.58	5.21–54.93
Asterorotalia pulchella	9.01	0–37.93	*Heterolepa dutemplei*	10.63	0–18.64	*Textularia* cf. *T. agglutinans*	10.26	2.79–19.28
Quinqueloculina adiazeta	8.33	0–50.00	*Textularia* sp. A	5.69	0–9.09	*Hanzawaia nipponica*	8.88	0–28.24
Cribroelphidium cf. *C. detense*	4.3	0–25.81	*Assilina ammonoides*	4.58	0–12.68	*Cavarotalia annectens*	7.79	3.62–18.01
Agglutinella agglutinans	3.64	0–13.79	*Hanzawaia nipponica*	4.39	0–9.18	*Heterolepa dutemplei*	4.73	0–14.01
Textularia haueri	2.77	0–8.33	*Textularia haueri*	3.39	0–8.5	*Elphidium* cf. *E. advenum*	4.3	1.43–9.32
Textularia sp. A	0.81	0–4.84	*Ammonia supera*	2.52	0–5.63	*Bigenerina nodosaria*	3.79	1.62–7.49
Elphidium sp.	0.7	0–3.45	*Parrellina hispidula*	2.39	0–8.11	*Pseudorotalia indopacifica*	2.57	0–8.14
Heterolepa dutemplei	0.67	0–3.23	*Pseudorotalia schroeteriana*	2.28	0–5.08	*Pseudorotalia schroeteriana*	2.55	0.90–4.56
Asterorotalia gaimardi	0.57	0–3.45	*Asterorotalia milletti*	2.23	0–7.28	*Quinqueloculina philippinensis*	1.9	0–5.92
Paracibicides edomica	0.57	0–3.45	*Agglutinella agglutinans*	2.18	0–5.41	*Cribroelphidium* cf. *C. detense*	1.87	0.90–5.00
Adelosina littoralis	0.27	0–1.61	*Quinqueloculina* sp.	2	0–4.5	*Triloculina tricarinata*	1.63	0.33–2.86
Ammonia supera	0.27	0–1.61	*Bigenerina nodosaria*	1.84	0–5.41	*Agglutinella agglutinans*	1.59	0.93–2.14
Bigenerina nodosaria	0.27	0–1.61	*Pseudorotalia indopacifica*	1.76	0–5.41	*Quinqueloculina incisa*	1.53	0–3.22
Elphidium indicum	0.27	0–1.61	*Asterorotalia gaimardi*	1.71	0–4.23	*Cancris auriculus*	1.03	0.31–2.25
Planispirinella exigua	0.27	0–1.61	*Ammonia tepida*	1.47	0–5.41	*Textularia* sp. A	1.01	0–6.81
Quinqueloculina incisa	0.27	0–1.61	*Elphidium* cf. *E. advenum*	1.19	0–5.14	*Asterorotalia milletti*	0.96	0–2.96
Quinqueloculina laevigata	0.27	0–1.61	*Ammonia convexa*	1.01	0–2.82	*Heterolepa subhaidingeri*	0.89	0–2.96
			Massilina cf. *M. planata*	0.93	0–4.23	*Parrellina hispidula*	0.76	0–2.25
			Reussella spinulosa	0.88	0–2.85	*Quinqueloculina adiazeta*	0.57	0–2.30
			Elphidium indicum	0.85	0–5.45			
			Quinqueloculina philippinensis	0.83	0–1.69			
			Elphidium jensoni	0.81	0–3.64			
			Heterolepa praecincta	0.81	0–5.08			
			Paracibicides edomica	0.77	0–5.41			
			Cylindroclavulina bradyi	0.66	0–2.22			
			Quinqueloculina incisa	0.64	0–1.82			
			Discorbinella bodjongensis	0.57	0–2.70			
			Eponides repandus	0.45	0–1.82			
			Cribroelphidium cf. *C. detense*	0.43	0–3.00			
			Proemassilina arenaria	0.43	0–1.69			
			Heterolepa subhaidingeri	0.42	0–3.39			
			Reophax sp.	0.42	0–3.39			
			Nubeculina divaricata	0.42	0–2.00			
			Quinqueloculina adiazeta	0.42	0–1.41			
			Planispirinella exigua	0.4	0–1.58			
			Spirotextularia floridana	0.4	0–1.5			
			Quinqueloculina lamarckiana	0.37	0–1.27			
			Triloculina tricarinata	0.36	0–1.47			
			Cibicides refulgens	0.35	0–2.82			
			Elphidium sp.	0.34	0–2.70			
			Discorbea candeiana	0.32	0–2.53			
			Ammonia cf. *A. takanabensis*	0.31	0–2.00			
			Quinqueloculina bicarinata	0.3	0–1.47			
			Reophax scorpiorus	0.28	0–2.21			
			Quinqueloculina parvaggluta	0.27	0–1.69			
			Cibicides sp.	0.24	0–1.41			
			Adelosina littoralis	0.16	0–0.5			
			Quinqueloculina laevigata	0.12	0–0.5			
			Triloculina trigonula	0.12	0–0.5			
			Lobatula lobatula	0.1	0–0.5			
			Quinqueloculina crassicarinata	0.06	0–0.45			
			Spirotextularia fistulosa	0.06	0–0.45			

F2A	Mean	Range	F2B	Mean	Range	F3	Mean	Range
24 Samples, 57 Taxa	%	%	16 Samples, 55 Taxa	%	%	25 samples, 26 taxa	%	%
Heterolepa dutemplei	14.65	1.20–22.14	*Heterolepa dutemplei*	11.31	4.46–14.75	*Heterolepa dutemplei*	13.11	4.74–21.75
Textularia sp. A	13.26	4.81–24.64	*Hanzawaia nipponica*	9.26	0.75–16.04	*Asterorotalia milletti*	11.73	2.28–21.86
Quinqueloculina incisa	4.65	0.33–7.53	*Textularia* sp. A	9.02	0.44–17.43	*Textularia* sp.A	9.36	0–28.57
Cylindroclavulina bradyi	4.12	0.64–11.11	*Quinqueloculina incisa*	6.88	2.84–12.01	*Hanzawaia nipponica*	7.27	4.05–10.39
Asterorotalia gaimardi	3.9	0–6.88	*Textularia haueri*	6.35	0–15.79	*Elphidium* cf. *E. advenum*	3.98	0.72–6.75
Hanzawaia nipponica	3.52	0.72–9.86	*Triloculina tricarinata*	5.61	0.75–10.32	*Sigmoilopsis schlumbergeri*	2.93	0–6.84
Agglutinella agglutinans	3.18	0–6.64	*Ammonia supera*	5.24	2.46–8.03	*Bigenerina nodosaria*	2.75	0–8.75
Ammonia supera	2.93	0–5.96	*Cylindroclavulina bradyi*	3.87	1.39–9.62	*Pseudorotalia indopacifica*	2.69	0–5.82
Textularia haueri	2.45	0–7.58	*Asterorotalia gaimardi*	3.41	0–8.03	*Quinqueloculina incisa*	2.57	0–13.01
Bigenerina nodosaria	2.38	0.81–4.74	*Agglutinella agglutinans*	2.57	0.42–10.87	*Ammonia* cf. *A. takanabensis*	2.31	0.62–6.12
Triloculina tricarinata	1.8	0–8.60	*Reussella spinulosa*	2.4	0–6.78	*Quinqueloculina lamarckiana*	1.96	0–4.44
Pseudorotalia indopacifica	1.74	0–4.76	*Bigenerina nodosaria*	2.34	0–4.37	*Triloculina tricarinata*	1.96	0–8.66
Spirotextularia floridana	1.7	0–3.10	*Pseudorotalia indopacifica*	1.77	0.35–4.00	*Textularia haueri*	1.85	0–4.43
Paracibicides edomica	1.67	0–7.06	*Cancris auriculus*	1.63	0–5.67	*Cancris auriculus*	1.82	0–4.69
Proemassilina arenaria	1.64	0.35–3.33	*Asterorotalia milletti*	1.33	0–2.71	*Pseudorotalia schroeteriana*	1.68	0–6.46

(*continued on next page*)

Table 6 (*continued*)

F2A	Mean	Range	F2B	Mean	Range	F3	Mean	Range
Quinqueloculina philippinensis	1.46	0–3.49	*Proemassilina arenaria*	1.09	0–2.71	*Asterorotalia gaimardi*	1.27	0–5.16
Asterorotalia milletti	1.45	0–5.28	*Elphidium* cf. *E. advenum*	1.04	0–2.94	*Ammonia convexa*	1.2	0–3.25
Quinqueloculina sp.	1.12	0–3.51	*Spirotextularia fistulosa*	1.02	0–4.24	*Nonion japonicum*	1.2	0–5.02
Nubeculina divaricata	1.09	0–4.18	*Quinqueloculina laevigata*	1.02	0–2.78	*Spirotextularia floridana*	1.04	0–2.96
Pseudorotalia schroeteriana	0.92	0–2.46	*Planispirinella exigua*	0.99	0–2.95	*Quinqueloculina philippinensis*	1.04	0–3.45
Spiroloculina communis	0.85	0–2.00	*Quinqueloculina philippinensis*	0.97	0–2.46	*Cavarotalia annectens*	0.91	0–4.18
Quinqueloculina laevigata	0.79	0–3.24	*Ammonia convexa*	0.88	0.34–1.47	*Thurammina* sp. A	0.8	0–7.11
Ammonia convexa	0.74	0–2.71	*Adelosina littoralis*	0.81	0–2.21	*Quinqueloculina bicarinata*	0.37	0–2.37
Quinqueloculina parvaggluta	0.68	0–3.33	*Spirotextularia floridana*	0.74	0–1.84	*Spiroloculina manifesta*	0.34	0–2.08
Reussella spinulosa	0.67	0–2.22	*Pyrgoella tenuiaperta*	0.71	0–2.96	*Triloculina trigonula*	0.23	0–4.79
Elphidium cf. *E. advenum*	0.66	0–2.00	*Triloculinella pseudooblonga*	0.66	0–2.06	*Nonion subturgidum*	0.19	0–2.17
Discorbia candeiana	0.65	0–4.30	*Elphidium indicum*	0.6	0–2.06			
Cancris auriculus	0.57	0–1.57	*Pseudorotalia schroeteriana*	0.59	0–2.09			
Eponides repandus	0.54	0–2.02	*Nubeculina divaricata*	0.51	0–3.76			
Adelosina littoralis	0.49	0–1.59	*Ammonia* cf. *A. takanabensis*	0.48	0–2.06			
Quinqueloculina lamarckiana	0.46	0–1.53	*Parrellina hispidula*	0.47	0–1.78			
Discorbinella bodjongensis	0.43	0–2.11	*Eponides repandus*	0.47	0–1.37			
Quinqueloculina bicarinata	0.41	0–2.22	*Quinqueloculina lamarckiana*	0.46	0–2.13			
Quinqueloculina adiazeta	0.39	0–2.22	*Paracibicides edomica*	0.46	0–2.22			
Spirotextularia fistulosa	0.38	0–1.15	*Discorbia candeiana*	0.42	0–1.09			
Reophax sp.	0.32	0–1.91	*Spiroloculina communis*	0.41	0–1.20			
Pyrgoella tenuiaperta	0.3	0–1.79	*Quinqueloculina* sp.	0.4	0–1.61			
Lobatula lobatula	0.25	0–4.74	*Cibicides* sp.	0.36	0–3.56			
Quinqueloculina crassicarinata	0.25	0–2.33	*Triloculina trigonula*	0.33	0–1.48			
Triloculinella pseudooblonga	0.23	0–1.62	*Quinqueloculina adiazeta*	0.33	0–1.33			
Assilina ammonoides	0.23	0–2.33	*Quinqueloculina parvaggluta*	0.29	0–1.18			
Cibicides sp.	0.22	0–1.60	*Quinqueloculina bicarinata*	0.29	0–1.27			
Ammonia cf. *A. takanabensis*	0.2	0–2.54	*Discorbinella bodjongensis*	0.27	0–1.39			
Triloculina trigonula	0.15	0–2.61	*Asterorotalia pulchella*	0.23	0–1.61			
Planispirinella exigua	0.14	0–1.43	*Ammonia tepida*	0.15	0–0.54			
Spiroloculina depressa	0.12	0–2.20	*Massilina* cf. *M. planata*	0.07	0–0.84			
Elphidium sp.	0.11	0–2.72	*Elphidium jensoni*	0.06	0–0.34			
Heterolepa subhaidingeri	0.11	0–1.05	*Reophax* sp.	0.05	0–0.44			
Massilina cf. *M. planata*	0.07	0–0.38	*Heterolepa praecincta*	0.03	0–0.40			
Heterolepa praecincta	0.07	0–0.63	*Assilina ammonoides*	0.02	0–0.40			
Elphidium indicum	0.06	0–0.73	*Quinqueloculina crassicarinata*	0.02	0–0.37			
Cibicides refulgens	0.05	0–0.39	*Elphidium* sp.	0.02	0–0.34			
Asterorotalia pulchella	0.03	0–0.47	*Heterolepa subhaidingeri*	0.02	0–0.34			
Parrellina hispidula	0.03	0–0.35	*Cibicides refulgens*	0.02	0–0.29			
Elphidium jensoni	0.02	0–0.40	*Spiroloculina depressa*	0.02	0–0.29			
Ammonia tepida	0.01	0–0.33						
Cribroelphidium cf. *C. detense*	0.01	0–0.33						

and recognized it in several incised valleys along the northern Gulf of Mexico margin. They attributed the overfilling to the size of the drainage basin and to climate change during the glacial-interglacial transition (from more arid to more humid). Both of these factors are likewise important in our study area. Degree of fill should also vary inversely as a function of the rate of transgression (Dalrymple, 2006), thus given the very low gradient of the shelf and resulting rapid transgression, very high rates of sedimentation are implied. The paleo-Chao Phraya incised valley could also be classified as overfilled in the terminology of Simms et al. (2006). However, the origin of most of the fill described by Alqahtani et al. (2015, 2017) is unclear (meandering fluvial to heterolithic units containing shells).

Given the sequence stratigraphic interpretation developed above, the environmental evolution of this shelf during the most recent base-level rise may be assessed. Earliest recovered deposits date from the Younger Dryas interval (12.8–11.7 ka; Rasmussen et al., 2006). This unit was encountered only at bottom of one core (Unit 2, GC16B) on the western side of the paleo-Chao Phraya River valley (Figs. 1B, 3), and we did not recover the base. Based on the foraminifera and sediments, the likely setting is that of the paleo-Chao Phraya river valley serving as a wide, shallow, low energy open embayment. At this time, the shoreline would have coincided with the western margin of the paleo-Chao Phraya River valley. With relative sea-level at −65 m, the shelf to the west of the valley was still subaerially exposed. As sea-level rose, the embayment transitioned to an open shelf setting, and shoreline erosion occurred along the western margin of the valley, exposing the underlying late Pleistocene unit (Unit 1) at GC8A, and creating a transgressive ravinement surface (TRS) (Figs. 3, 13).

The present inner shelf (landward of the 60 m isobath; Fig. 1B) was flooded at approximately 12,000 cal y BP. Given high rates of sea-level rise at this time (Fig. 2; Hanebuth et al., 2011), the shoreline would have transgressed rapidly, with deposition occurring in wetland environments of the paleo-Marang and Terengganu river valleys by ca. 11,600 cal yr BP and offshore (organic-rich muds in GC14B; Figs. 1B, 3) on the eastern flank of the paleo-Chao Phraya River valley. As shelf waters deepened and the shoreline transgressed, the transgressive ravinement surface (TRS) shifted to the region of GC11B by at least ca. 11,000 cal yr BP (Fig. 13). As the TRS continued to shift westward along with the shoreline, shallow inner shelf sediments with a low diversity foraminiferal assemblage transitioned to deeper water, higher diversity assemblages within the paleo-Chao Phraya river valley, forming the upper portion (above the TRS) of the transgressive systems tract (TST) (Figs. 3, 13). These TST deposits correlate with the transgressive unit described by Evans et al. (1995) and Hanebuth and Stattegger (2003), i.e., a

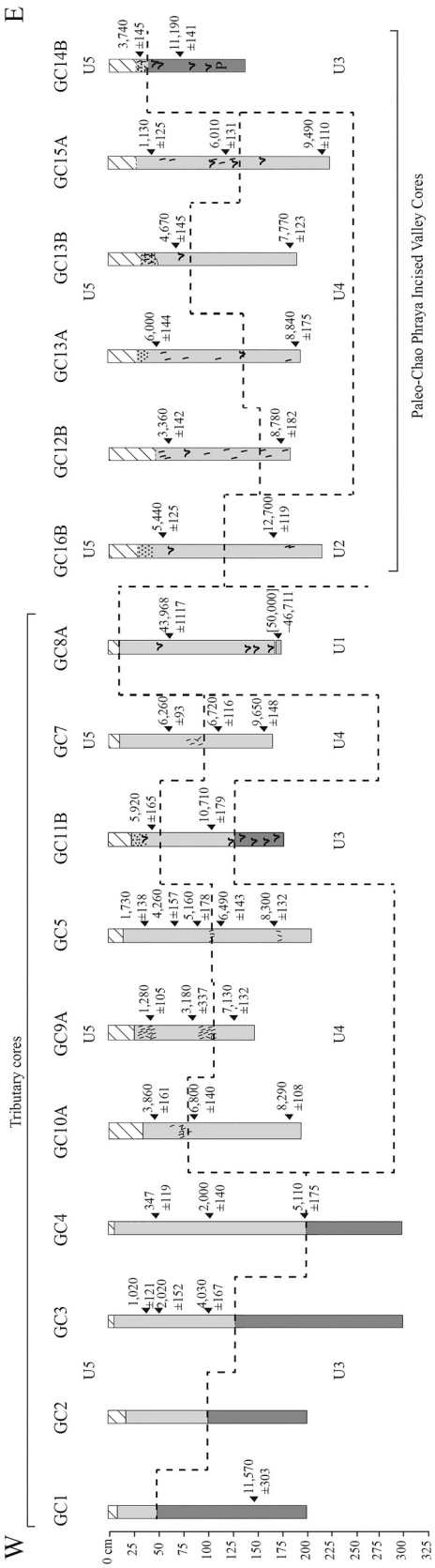

Fig. 12. West to east section of 16 core logs, showing radiocarbon age estimates and chronostratigraphic Units 1–5. See Fig. 1 for location of cores on the Sunda Shelf. See Fig. 4 for key to core log symbols.

succession of terrestrial to shoreline to marine deposits underlain by a subaerial to submarine discontinuity.

With continued transgression, the shoreline (and TRS) shifted inland of the modern shoreline at ca. 7000–6500 cal yr BP. This marks the timing of the maximum flooding surface (MFS Loutit et al., 1988) across the shelf in this area (transition from Unit 4 to Unit 5) (Figs. 3, 13). Continued flux of sediments to coastal regions and the inner shelf via the Marang and Terengganu rivers, and the minor relative sea-level fall (1.3–3 m; Hanebuth et al., 2011; Mallinson et al., 2014; Parham et al., 2014; Bradley et al., 2016), from 6500 cal yr BP to near present, built the coastal system seaward, and allowed continued deposition on the shelf, forming the highstand systems tract (HST) (Figs. 3, 13). The primary indicators of the occurrence of the HST are the increase (across the MFS) in the number of planktonic foraminifera and wt% Ca, and the decrease in the BMS, and wt% Al and Fe.

6. Summary

The sediments in cores collected over the paleo-Chao Phraya River and paleo-Terengganu and paleo-Marang incised river valleys are geologically consistent with the findings of Hanebuth and Stattegger (2003), Hanebuth et al. (2011) and several other authors (see Sathiamurthy and Rahman, 2017) and exhibit a 2–3 m thick Holocene section characterized by foraminiferal-rich mud to sandy mud (Hanebuth et al., 2011; this study). Using a multi-proxy approach (geochronology, bulk sediment magnetic susceptibility, elemental analysis, and foraminiferal assemblages), five late Pleistocene to Holocene chronostratigraphic units are recognized on the western Sunda Shelf. Unit 1 is an inner shelf deposit that is much older than other units and dates from a Pleistocene sea-level highstand. Unit 2 was deposited as part of the most recent base-level cycle and is a late Pleistocene (Younger Dryas) shallow open embayment deposit associated with the inundation of the paleo-Chao Phraya River valley. Unit 3 consists of a late Pleistocene to early Holocene paralic peat deposit on the current inner shelf and organic-rich muds farther seaward. Units 1, 2, and 3 form the "basement" upon which two entirely Holocene marine units (Unit 4 and 5) were deposited. Unit 4 was deposited during the early Holocene transgression on the Sunda Shelf and Unit 5 was deposited ca. 6500 cal yr BP (during the regional sea-level highstand) to present.

A sequence stratigraphic interpretation of the cores collected on the Sunda shelf and, with comparison to regional sea-level curves, supports the following:

1. As RSL rose and the shelf was inundated (post-LGM; ca. 21,000 cal yr BP to 11,200 cal yr BP), fluvial sediments (inferred) were replaced by shallow shelf embayment muds and paralic peaty muds.
2. At ca. 11,500 cal y BP paralic sediments transition upward and landward to open shelf foraminifera-rich mud, still with significant terrestrial influence. These paralic and open shelf deposits represent the transgressive systems tract (TST).
3. The maximum flooding surface is dated at ca. 6500 cal yr BP. It is overlain by foraminifera-rich mud of the highstand systems tract (HST) (1–1.5 m thick) and is characterized by less terrestrial influence during deposition than the TST deposits.
4. Coastal plain deposits exposed during lowstand conditions, which formed positive topography during the Holocene sea-level rise, are currently covered by <50 cm of Holocene marine sediment on interstream divides between tributaries of the paleo-Chao Phraya River.
5. High sediment accumulation rates during post-LGM sea-level rise within incised valleys resulted in minimal accommodation space for Holocene marine sediments (i.e., valleys are filled primarily with late Pleistocene fluvial to paralic sediments). These valleys may be considered overfilled as a result of the generally high fluvial sediment flux associated with humid tropical and monsoon conditions. The difference in thickness of marine sediments in valleys compared

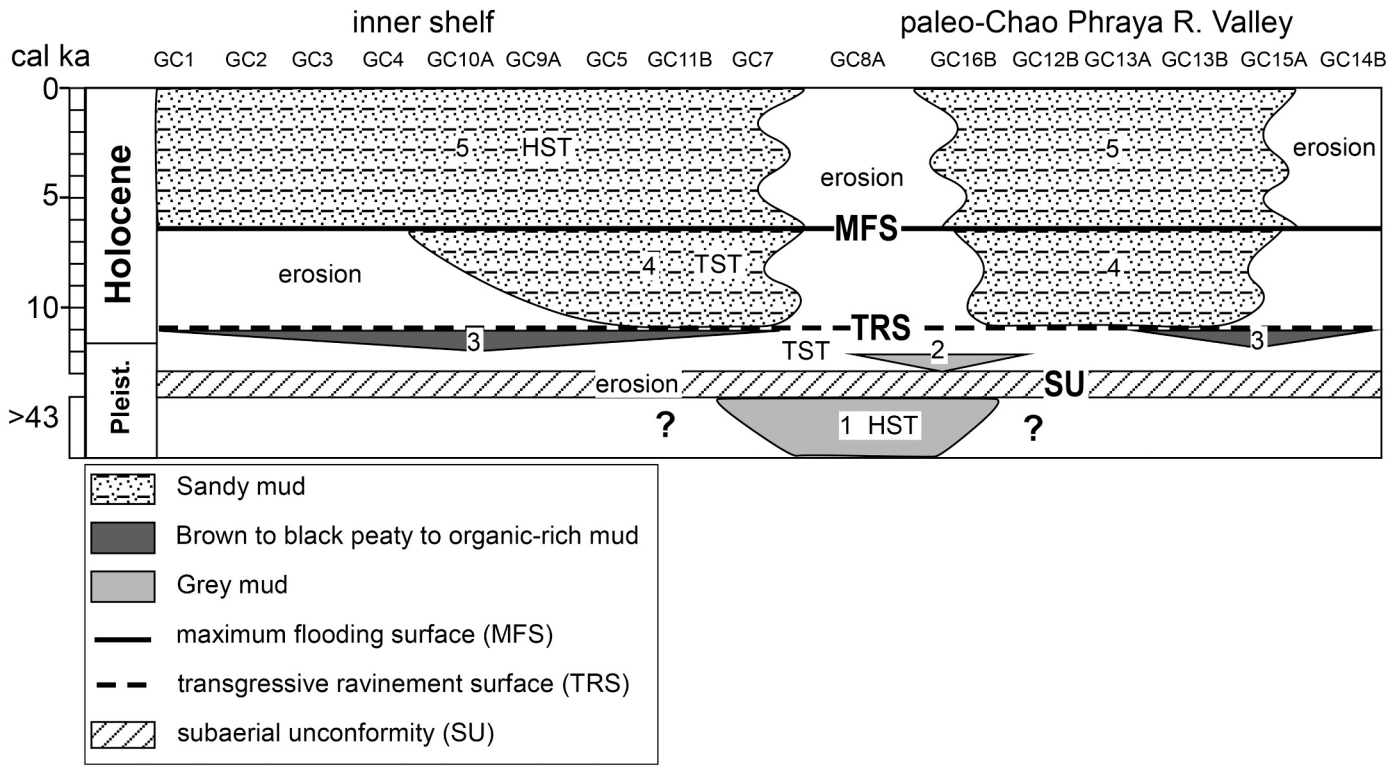

Fig. 13. Chronostratigraphic diagram showing horizontal and vertical distribution of late Pleistocene to Holocene Units 1–5, the transgressive ravinement surface and the maximum flooding surface. The subaerial unconformity was formed during the LGM. Note the break in vertical scale. The spatial extent of Unit 1 is not known as it was only recovered in one core (GC8A).

to the adjacent shelf is minimal: <1 m on the shelf and 2–3 m in/above the Terengganu and Marang valleys. The exception may be in the paleo-Chao Phraya incised valley, where we did not recover the base of the open shelf transgressive unit (Unit 4). There may yet be a thicker unit of shelf marine sediments here, as suggested by Alqahtani et al. (2015).

Supplementary data to this article can be found online at https://doi.org/10.1016/j.margeo.2021.106457.

Declaration of Competing interest

The authors declare that they have no known competing financial interests or personal relationships that could have appeared to influence the work reported in this paper.

Acknowledgements

We thank the captains and crew of the *RV Discovery* and *RV Discovery II*, Institute of Oceanography and Environment (INOS) technicians, and Universiti Malaysia Terengganu graduate students for support at sea and in the laboratory. Special thanks go to Joseph Bidai, Mohd Zulkamal Mohd Rahzi, Tan Hock Seng, Che Mohd Kamarul Anuar, Fathullah Abdullah, Mohd Arif Shamsuri, Mohd Harris Sakri, Mohd Fakarullah, Khoo Siao Jean, Dr. Fatin Minhat, and Dr. Adiana Ghazali. We thank John Woods, Jim Watson, Kim West, Dare Merritt, students Nina Shmorhun, Sam Martin, Caroline Smith, Seth Sutton, Jessica Kegel, and C.J. Whitley for support at ECU. We thank Dr. David Menier for sharing the results of his geophysical surveys off Kuala Terengganu and Dr. Faisal Alqahtani for input on core location. Acknowledgement is made to East Carolina University and Universiti Malaysia Terengganu for support and to the National Science Foundation for grant OISE-1157222.

References

Ahmad, M.F., Goh, S., Wan Nik, W.M.N., Jamaluddin, N., 2009. Study on the distribution characteristics of sediments at the estuary and along the Kuala Terengganu River. In: Second International Conference on Environmental and Computer Science, pp. 303–308. https://doi.org/10.1109/ICECS.2009.54.

Alqahtani, F.A., Johnson, H.D., Jackson, C.A.-L., Som, R.B., 2015. Nature, origin and evolution of a late Pleistocene incised valley-fill, Sunda Shelf, Southeast Asia. Sedimentology 62, 1198–1232.

Alqahtani, F.A., Jackson, C.A.-L., Johnson, H.D., Som, R.B., 2017. Controls on the geometry and evolution of humid-tropical fluvial systems: insights from 3D seismic geomorphological analysis of the Malay Basin, Sunda Shelf, Southeast Asia. J. Sediment. Res. 87, 17–40.

Azmi, N., Minhat, F.I., Hasan, S.S., Rahman, A.M., A'ziz, A.N., Saelan, W.N.W., Shaari, H., Aziz, A.A., Suratman, S., 2020. Distribution of benthic Foraminifera off Kelantan, peninsular Malaysia, South China Sea. J. Foraminifer. Res. 50, 89–95.

Bahr, A., Lamy, F., Arz, H., Kuhlmann, H., Wefer, G., 2005. Late glacial to Holocene climate and sedimentation history in the NW Black Sea. Mar. Geol. 214, 309–322.

Bird, M., Fifield, L., The, T., Chang, C., Shirlaw, N., Lambeck, K., 2007. An inflection in the rate of early mid-Holocene eustatic sea-level rise: a new sea-level curve from Singapore. Estuar. Earth Planet. Sci. Lett. Coast. Shelf Sci. 71, 523–536.

Biswas, B., 1976. Bathymetry of Holocene Foraminifera and Quaternary sea-level changes on the Sunda Shelf. J. Foraminifer. Res. 6, 107–133.

Boyd, R., Dalrymple, R.W., Zaitlin, B.A., 2006. Estuarine and incised-valley facies models. SEPM Spec. Publ. 84, 171–235.

Bradley, S., Milne, G., Horton, B., Zong, Y., 2016. Modelling sea level data from China and Malay-Thailand to estimate Holocene ice-volume equivalent sea level change. Quat. Sci. Rev. 137, 54–68.

Buzas, M.A., 1979. The measurement of species diversity. In: Lipps, Jerry H. (Ed.), Foraminiferal Ecology and Paleoecology: Society of Economic Paleontologists and Mineralogists, Short Course, 6, pp. 3–10.

Clark, P.U., Dyke, A.S., Shaku, J.D., Carlson, A., Clark, J., Wohlfarth, B., Mitrovica, J., Hostetler, S.W., McCabe, A.M., 2009. The last glacial maximum. Science 325, 710–714.

Culver, S.J., Mallinson, D.J., Corbett, D.R., Leorri, E., Rouf, A., Shazili, N.A.M., Yaacob, R., Whittaker, J.E., Buzas, M.A., Parham, P.R., 2012. Distribution of foraminifera in the Setiu estuary and lagoon, Terengganu, Malaysia. J. Foraminifer. Res. 42, 109–133.

Culver, S.J., Leorri, E., Corbett, D.R., Mallinson, D.J., Shazili, N.A.M., Nasir, M., Parham, P.R., Rosnan, Y., 2013. Infaunal mangrove swamp foraminifera in the Setiu wetland, Terengganu, Malaysia. J. Foraminifer. Res. 43, 262–279.

Culver, S.J., Leorri, E., Mallinson, D.J., Corbett, D.R., Shazili, N.A.M., 2015. Recent coastal evolution and sea-level rise, Setiu wetland, peninsular Malaysia. Palaeogeogr. Palaeoclimatol. Palaeoecol. 417, 406–421.
Dalrymple, R.W., Zaitlin, B.A., Boyd, R., 1992. Estuarine facies models: conceptual basis and stratigraphic implications. J. Sediment. Petrol. 62, 1130–1146.
Dalrymple, R.W., Boyd, R., Zaitlin, B.A., 1994. Incised-valley systems: origin and sedimentary sequences. SEPM Spec. Publ. 51, 391 p.
Dalrymple, R.W., 2006. Incised valleys in time and space: An introduction to the volume and an examination of the controls on valley formation and filling. In: Dalrymple, R. W., Leckie, D.A., Tillman, R.W. (Eds.), Incised Valleys in Time and Space, SEPM Spec. Publ., 85, pp. 5–12.
Darmadi, Y., Willis, B.J., Dorobek, S.L., 2007. Three-dimensional seismic architecture of fluvial sequences on the low-gradient Sunda Shelf, offshore Indonesia. J. Sediment. Res. 77, 224–238.
Emmel, F.J., Curray, J.R., 1982. A Submerged late Pleistocene delta and other features related to sea level changes in the Malacca Strait. Mar. Geol. 47, 192–216.
Evans, C.D.R., Brett, C.P., James, J.W.C., Holmes, R., 1995. Shallow seismic reflection profiles from the waters of East and Southeast Asia: an interpretation manual and atlas. In: British Geological Survey, Technical Report WC/94/60, pp. 66–67.
Fairbanks, R., 1989. A 17,000-year glacio-eustatic sea level record: influence of glacial melting rates on the Younger Dryas event and deep-ocean circulation. Nature 342, 637–642.
Geyh, M., Kudrass, H., Streif, H., 1979. Sea-level changes during the Late Pleistocene and Holocene in the Strait of Malacca. Nature 278, 441–443.
Graham, J.J., Militante, P.J., 1959. Recent foraminifera form the Puerto Galera area, northern Mindoro, Philippines. Stanford University Publications. Geol. Sci. 6, 1–171.
Haig, D.W., 1988. Miliolid foraminifera from inner neritic sand and mud facies of the Papuan Lagoon, New Guinea. J. Foraminifer. Res. 18, 203–236.
Hanebuth, T.J.J., Stattegger, K., 2003. The stratigraphic evolution of the Sunda Shelf during the past fifty thousand years. In: Sidi, F.H., Nummedal, D., Imbert, P., Darman, H., Posamentier, H.W. (Eds.), Tropical Deltas of Southeast Asia - Sedimentology, Stratigraphy, and Petroleum Geology, Society of Economic Paleontologists and Mineralogists, Special Publication, Vol. 76, pp. 189–200.
Hanebuth, T.J.J., Stattegger, K., Grootes, P.M., 2000. Rapid flooding of the Sunda Shelf: a late-glacial sea-level record. Science 288, 1033–1035.
Hanebuth, T.J.J., Stattegger, K., Bojanowski, A., 2009. Termination of the Last Glacial Maximum sea-level lowstand: the Sunda Shelf sea-level record revisited. In: Camoin, G., Droxler, A., Miller, K., Fulthorpe, C. (Eds.), Records of Quaternary Sea-Level Changes, Global and Planetary Change, Vol. 66, pp. 76–84.
Hanebuth, T.J.J., Voris, H.K., Yokoyama, Y., Saito, Y., Okuno, J., 2011. Formation and fate of sedimentary depocentres on Southeast Asia's Sunda Shelf over the past sea-level cycle and biogeographic implications. Earth Sci. Rev. 104, 92–110.
Hesp, P., Hung, C., Hilton, M., Ming, C., Turner, I., 1998. A first tentative Holocene sea-level curve for Singapore. J. Coast. Res. 14, 308–314.
Horton, B., Gibbard, P., Milne, G., Morley, R., Purintavaragual, C., Stargardt, J., 2005. Holocene sea levels and paleoenvironments, Malay-Thai Peninsula Southeast Asia. The Holocene 15, 1199–1213.
Jones, R.W., 1994. The Challenger Foraminifera. Oxford University Press, London.
Lee, H.L., Tangang, F., Gisen, J.I., Suratman, S., 2017. Prediction of salinity intrusion in the sheltered estuary of Terengganu River in Malaysia using 1-D empirical intrusion model. Acta Oceanol. Sin. 36, 57–66.
Loeblich Jr., A.R., Tappan, H., 1987. Foraminiferal Genera and their Classification. Van Nostrand Reinhold Company, New York.
Loeblich Jr., A.R., Tappan, H., 1994. Foraminifera of the Sahul Shelf and Timor Sea. Cushman Found. Foram. Res. Spec. Publ. 31, 1–638.
Loutit, T.S., Harbenbol, J., Vail, P.R., Baum, G.R., 1988. Condensed sections: the key to age determination and correlation of continental margin sequences. SEPM Spec. Publ. 42, 118–213.
Mallinson, D.J., Culver, S.J., Corbett, D.R., Parham, P.R., Shazili, N.A.M., Yaacob, R., 2014. Holocene coastal response to monsoons and relative sea-level changes in northeast peninsular Malaysia. J. Asian Earth Sci. 91, 194–205.
Mansor, M.Y., Rahman, A.H.A., Menier, D., Pubellier, M., 2014. Structural evolution of Malay Basin, its links to Sunda Block tectonics. Mar. Pet. Geol. 58, 736–748.
Martin, S.Q., Culver, S.J., Leorri, E., Mallinson, D.J., Buzas, M.A., Hayek, L.A.C., Shazili, N.A.M., 2018. Distribution and taxonomy of modern benthic foraminifera of the Western Sunda Shelf (South China Sea) off Peninsular Malaysia. Cushman Found. Foram. Res. Spec. Publ. 31, 1–112.
McGann, M., Erikson, L., Wan, E., Powell II, C., Maddocks, R.F., 2013. Distribution of biologic, anthropogenic, and volcanic constituents as a proxy for sediment transport in the San Francisco Bay Coastal System. Mar. Geol. 345, 113–142.
Mello, J., Buzas, M.A., 1968. An application of cluster analysis as a method of determining biofacies. J. Paleontol. 42, 747–758.
Miall, A.D., 2002. Architecture and sequence stratigraphy of Pleistocene fluvial systems in the Malay Basin, based on seismic time-slice analysis. Am. Assoc. Pet. Geol. Bull. 86, 1201–1216.
Michel, G.W., Becker, M., Angermann, D., Reigber, C., Reinhart, E., 2000. Crustal motion in E- and SE-Asia from GPD measurements. Earth Planets and Space 52, 713–720.
Milliman, J.D., Farnsworth, K.L., Albertin, C.S., 1999. Flux and fate of fluvial sediments leaving large islands in the East Indies. J. Sea Res. 41, 97–107.
Minhat, F., Satyanarayana, B., Husain, M., Rajan, V., 2016. Modern benthic foraminifera in subtidal waters of Johor: implications for Holocene sea-level change on the east coast of peninsular Malaysia. J. Foraminifer. Res. 46, 347–357.
Molengraaff, G.A.F., 1921. Modern deep-sea research in the East Indian archipelago. Geogr. J. 57, 95–121.
Molengraaff, G.A.F., Weber, M., 1921. On the relation between the Pleistocene glacial period and the origin of the Sunda Sea (Java and South China Sea), and its influence on the distribution of coral reefs and on the land and freshwater fauna. In: Proceedings, Royal Academy of Amsterdam. Vol. XXIII, Communicated at the Meeting of Nov. 29, 1919, pp. 395–439.
Parham, P.R., 2016. Late Cenozoic relative sea-level highstand record from peninsular Malaysia and Malaysian Borneo: implications for vertical crustal movements. Bull. Geol. Soc. Malaysia 62, 91–115.
Parham, P.R., Saito, Y., Sapon, N., Suriadi, R., Mohtar, N., 2014. Evidence for ca. 7-ka maximum Holocene transgression on the peninsular Malaysia east coast. J. Quat. Sci. 29, 414–422.
Pelejero, C., Kienast, M., Wang, L., Grimalt, J., 1999. The flooding of Sundaland during the last deglaciation: imprints in hemipelagic sediments from the southern South China Sea. Earth Planet. Sci. Lett. 171, 661–671.
Posamentier, H.W., 2001. Lowstand alluvial bypass systems: incised vs. unincised. Am. Assoc. Pet. Geol. Bull. 85, 1771–1793.
Puchala, R.J., Porebski, S.J., Sliwinski, W.R., August, C.J., 2011. Pleistocene to Holocene transition in the central basin of the Gulf of Thailand, based on geoacoustic survey and radiocarbon ages. Mar. Geol. 288, 103–111.
Rahman, M.M., Sathiamurthy, E., Zhong, G., Geng, J., Liu, Z., 2016. CHIRP acoustic characterization of paleo fluvial system of late-Pleistocene to Holocene in Penyu Basin, Sunda Shelf. Bull. Geol. Soc. Malaysia 62, 47–56.
Rasmussen, S.O., Andersen, K.K., Svensson, A.M., Steffensen, J.P., Vinther, B.M., Clausen, H.B., Siggaard-Andersen, M.-L., Johnson, S.J., Larsen, L.B., Dahl-Jensen, D. , Bigler, M., Rothlisberher, R., Fischer, H., Goto-Azuma, K., Hansson, M.E., Ruth, U., 2006. A new Greenland ice core chronology for the last glacial termination. J. Geophys. Res. 111, D06102 https://doi.org/10.1029/2005JD006079.
Reijenstein, H.M., Posamentier, H.W., Bhattacharya, J.P., 2011. Seismic geomorphology and high-resolution seismic stratigraphy of inner-shelf fluvial, estuarine, deltaic and marine sequences, Gulf of Thailand. Am. Assoc. Pet. Geol. Bull. 95, 1959–1990.
Reimer, P.J., Bard, E., Bayliss, A., Beck, J.W., Blackwell, P.G., Ramsey, C.B., Buck, C.E., Cheng, H., Edwards, R.L., Friedrich, M., Grootes, P.M., Guilderson, T.P., Haflidason, H., Hajda, I., Hatte, C., Heaton, T.J., Hoffman, D.L., Hogg, A.G., Hughen, K.A., Kaiser, K.F., Kromer, B., Manning, S.W., Niu, M., Reimer, R.W., Richards, D.A., Scott, E.M., Southon, J.R., Staff, R.A., Turney, C.S.M., Plicht, J., 2013. INTCAL13 and MARINE13 radiocarbon age calibration curves 0-50,000 years Cal BP. Radiocarbon 55, 1869–1887.
Sathiamurthy, E., Rahman, M.M., 2017. Late Quaternary paleo fluvial system research of Sunda Shelf: a review. Bull. Geol. Soc. Malaysia 64, 81–92.
Sathiamurthy, E., Voris, H.K., 2006. Maps of Holocene sea level transgression andatg submerged lakes on the Sunda Shelf. Nat. Hist. J. Chulalongkorn Univ. Suppl. 2, 1–44.
Sen Gupta, B.K., 1999. Foraminifera in marginal marine environments. In: Sen Gupta, B. K. (Ed.), Modern Foraminifera. Kluwer Academic Publishers, Great Britain, pp. 141–159.
Simms, A.R., Anderson, J.B., Taha, Z.P., Rodriguez, A.B., 2006. Overfilled versus underfilled incised valleys: examples from the Quaternary Gulf of Mexico. SEPM Spec. Publ. 85, 117–139.
Simons, W.J.F., Socquet, A., Vigny, C., Ambrosius, B.A.C., Haji Abu, S., Promthong, C., Subarya, C., Sarsito, D.A., Matheussen, S., Morgan, P., Spakman, W., 2007. A decade of GPS in Southeast Asia: resolving Sundaland motion and boundaries. J. Geophys. Res. 112, B06420 https://doi.org/10.1029/2005JB003868.
Sorrel, P., Tessier, B., Demory, F., Baltzer, A., Bouaouina, F., Proust, J.-N., Menier, D., Traini, C., 2010. Sedimentary archives of the French Atlantic coast (inner Bay of Vilaine, South Brittany): depositional history and late Holocene climatic and environmental signals. Cont. Shelf Res. 30, 1250–1266.
Southon, J., Kashgarian, M., Fontugne, M., Metivier, B., Yim, W., 2002. Marine reservoir corrections for the Indian Ocean and Southeast Asia. Radiocarbon 44, 167–180.
Stuiver, M., Reimer, P.J., Reimer, R., 2017. Calib Radiocarbon Calibration Program, Version: Calib 7.1, United Kingdom. http://calib.qub.ac.uk/calib/calib.html.
Suriadi, R., Shaari, H., Culver, S.J., Husain, M.L., Rajan, V.V.V., Parham, P.R., Sapon, N. A., 2019. Inner shelf benthic foraminifera of the South China Sea, east coast peninsular Malaysia. J. Foraminifer. Res. 49, 11–28.
Szarek, R., 2001. Biodiversity and Biogeography of Recent Benthic Foraminiferal Assemblages in the South-Western South China Sea (Sunda Shelf). PhD dissertation. University of Kiel, pp. 1–273.
Szarek, R., Kuhnt, W., Kawamura, H., Kitazato, H., 2006. Distribution of recent benthic foraminifera on the Sunda Shelf (South China Sea). Mar. Micropaleontol. 61, 171–195.
Tanabe, S., Saito, Y., Sato, Y., Suzuki, Y., Sinsakul, S., Tiyapairoch, S., Chaimanee, N., 2003. Stratigraphy and Holocene evolution of the mud-dominated Chao Phraya delta, Thailand. Quat. Sci. Rev. 22, 789–807.
Tjallingii, R., Stattegger, K., Wetzel, A., Van Phach, P., 2010. In-filling and flooding of the Mekong River incised valley during deglacial sea-level rise. Quat. Sci. Rev. 29, 1432–1444.
Tjia, H.D., Liew, K.K., 1996. Changes in tectonic stress field in northern Sunda Shelf basins. In: Hall, R., Blundell, D. (Eds.), Tectonic Evolution of Southeast Asia, Geological Society Special Publication, Vol. 106, pp. 291–306.
Voris, H.K., 2000. Maps of Pleistocene Sea levels in Southeast Asia: shorelines, river systems and time durations. J. Biogeogr. 27, 1153–1167.
Wang, P., Wang, L., Bian, Y., Jian, Z., 1995. Late Quaternary paleoceanography of the South China Sea; surface circulation and carbonate cycles. Mar. Geol. 127, 145–165.
Wang, L., Sarnthein, M., Erlenkeuser, H., Grimalt, J., Grootes, P., Heilig, S., Ivanova, E., Klienast, M., Pelejero, C., Pflaumann, U., 1999. East Asian monsoon climate during the late Pleistocene; high-resolution sediment records from the South China Sea. Mar. Geol. 156, 245–284.

Wehausen, R., Brumsack, H., 2002. Astronomical forcing of the East Asian monsoon mirrored by the composition of Pliocene South China Sea sediments. Earth Planet. Sci. Lett. 201, 621–636.
Whittaker, J.E., Hodgkinson, R.L., 1979. Foraminifera of the Togopi Formation, eastern Sabah, Malaysia. Bulletin of the British Museum (Natural history). Geology 31, 1–120.
Woodson, A.L., Leorri, E., Culver, S.J., Mallinson, D.J., Parham, P.R., Thunell, R.C., Vijayan, V.R., Curtis, S., 2017. Sea-surface temperatures for the last 7200 years from the eastern Sunda Shelf, South China Sea: climatic inferences from planktonic foraminiferal Mg/Ca ratios. Quat. Sci. Rev. 165, 13–24.
Yu, K., Chen, T., 2009. Beach sediments from northern South China Sea suggest high and oscillating sea levels during the late Holocene. Earth Sci. Front. 16, 138–145.
Zaitlin, B.A., Dalrymple, R.W., Boyd, R., 1994. The stratigraphic organization of incised-valley systems associated with relative sea-level change. SEPM Spec. Publ. 51, 45–60.